

Structured Gene-Environment Interaction Analysis

Mengyun Wu^{1,3}, Qingzhao Zhang², Shuangge Ma³

¹School of Statistics and Management, Shanghai University of Finance and Economics

²School of Economics and Wang Yanan Institute for Studies in Economics, Xiamen University

³Department of Biostatistics, Yale University

email: shuangge.ma@yale.edu

Abstract

For the etiology, progression, and treatment of complex diseases, gene-environment (G-E) interactions have important implications beyond the main G and E effects. G-E interaction analysis can be more challenging with the higher dimensionality and need for accommodating the “main effects, interactions” hierarchy. In the recent literature, an array of novel methods, many of which are based on the penalization technique, have been developed. In most of these studies, however, the structures of G measurements, for example the adjacency structure of SNPs (attributable to their physical adjacency on the chromosomes) and network structure of gene expressions (attributable to their coordinated biological functions and correlated measurements), have not been well accommodated. In this study, we develop the structured G-E interaction analysis, where such structures are accommodated using penalization for both the main G effects and interactions. Penalization is also applied for regularized estimation and selection. The proposed structured interaction analysis can be effectively realized. It is shown to have the consistency properties under high dimensional settings. Simulations and the analysis of GENEVA diabetes data with SNP measurements and TCGA melanoma data with gene expression measurements demonstrate its competitive practical performance.

Keywords: G-E interaction; Structured analysis; High-dimensional modeling.

1 Introduction

Beyond the main genetic (G) and environmental (E) effects, gene-environment (G-E) interactions have been shown to be fundamentally important for the etiology, progression, prognosis, and response to treatment of many complex diseases. In the past decade, a long array of statistical methods have been developed for G-E interaction analysis and can be roughly classified as marginal analysis (under which one G measurement is analyzed at a time) and joint analysis (under which a large number of G measurements are analyzed in a single model). For relevant discussions, we refer to Thomas (2010); Wu et al. (2015); Wu and Ma (2018); Shim et al. (2018) and other published

studies. Compared to marginal analysis, joint analysis may better describe disease biology (that is, phenotypes and outcomes of complex diseases are associated with the combined effects of multiple genetic factors) and have attracted extensive attention in recent literature.

Joint G-E interaction analysis is challenging with the high data dimensionality. For estimation and also to screen out noises and identify important G-E interactions and main G effects, regularized estimation has been routinely conducted. Among the available techniques, penalization has been adopted in many of the recent studies. See Wu et al. (2015); Wu and Ma (2018) and references therein. Another challenge comes from the need to respect the “main effects, interactions” hierarchy (Bien et al., 2013; Hao and Zhang, 2017; Hao et al., 2018; She et al., 2018). Under the context of G-E interaction analysis with low-dimensional E variables, this hierarchy postulates that an interaction term cannot be identified, if the corresponding main G effect is not identified. With this hierarchy, “straightforward” penalizations are insufficient. Several penalization techniques have been developed in recent literature to respect this hierarchy (Liu et al., 2013; Wu et al., 2018).

A common limitation shared by many of the existing G-E interaction studies is that the structures of G measurements have not been well accounted for. Consider for example single nucleotide polymorphism (SNP) data. When SNPs are densely measured, those physically close are often in high linkage disequilibrium (LD) and likely to have similar biological functions or statistical effects (Reich et al., 2001). Here, there is an adjacency structure which arises from the physical adjacency of SNPs on chromosomes. As another example, consider gene expressions. Recent studies have shown that with coordinated biological functions and correlated measurements, gene expressions can be effectively described using a network structure (Barabasi et al., 2011). More details are provided below. Note that for other types of omics measurements, there are also underlying structures, although the construction of such structures may vary across data types.

In the high-dimensional analysis of main G effects, a few structured analysis approaches have been developed to accommodate the underlying structures in estimation and selection. Consider

the adjacency structure of SNPs (and other densely measured G factors). Available penalization approaches include the fused lasso (Tibshirani et al., 2005), smooth lasso (Hebiri and van de Geer, 2011), smoothed group lasso (Liu et al., 2012), spline lasso (Guo et al., 2016), and others. When gene expressions (and other G measurements) are described using network structures, network-constrained regularized estimation has been proposed (Michailidis, 2012). A popular approach is the network Laplacian-based penalization (Li and Li, 2008). Other network-structured penalization methods include the adaptive network-constrained regularization (Li and Li, 2010), TLP-based penalty for groups of indicators (Kim et al., 2013), sparse regression incorporating graphical structures among predictors (SRIG) (Yu and Liu, 2016), and others. Extensive investigations have shown that structured analysis can lead to more accurate and more interpretable identification and estimation of important effects. It is noted that, with similar spirits, structured analysis can also be conducted based on techniques other than penalization. As penalization is adopted in this study, the above literature review has been focused on this specific technique.

In this study, our goal is to conduct structured G-E interaction analysis, under which the structures of G measurements can be effectively accounted for. This has been well motivated by the success of structured analysis in the study of main G effects and a lack of such analysis in G-E interaction analysis. It is noted that this study is much more than a simple extension of the main-G-effect structured analysis. Specifically, in G-E interaction analysis, one G factor manifests multiple effects: its main effect as well as multiple E-interactions. The underlying structures need to be accounted for in the analysis of all these effects. This is further complicated by the “main effects, interactions” hierarchy. As a result, significant computational and statistical developments are needed. Also advancing from some of the existing studies, in this study, we accommodate multiple types of underlying structures under one framework. This unity significantly benefits methodological and statistical developments. Another advancement is that statistical properties are carefully established, which can provide a more solid ground than in some of the existing

studies. Overall, this study can provide an alternative and more effective way for conducting G-E interaction analysis.

2 Methods

Consider a dataset with n iid subjects. For the i th subject, let Y_i be the response of interest, and $\mathbf{Z}_i = (Z_{i1}, \dots, Z_{iq})$ and $\mathbf{X}_i = (X_{i1}, \dots, X_{ip})$ be the q - and p -dimensional vectors of E and G measurements. First, consider the scenario with a continuous outcome and a linear regression model with the joint effects of all E and G effects and their interactions:

$$Y_i = \sum_{k=1}^q Z_{ik}\alpha_k + \sum_{j=1}^p X_{ij}\beta_j + \sum_{k=1}^q \sum_{j=1}^p Z_{ik}X_{ij}\eta_{kj} + \varepsilon_i, \quad (1)$$

where α_k 's, β_j 's, and η_{kj} 's are the regression coefficients for the main E, main G, and their interactions, respectively, and ε_i 's are the random errors. We omit the intercept term to simplify notation.

To conveniently respect the ‘‘main effects, interactions’’ hierarchical constraint, we conduct the decomposition of η_{kj} as $\eta_{kj} = \beta_j\gamma_{kj}$. Then model (1) can be rewritten as

$$\begin{aligned} Y_i &= \sum_{k=1}^q Z_{ik}\alpha_k + \sum_{j=1}^p X_{ij}\beta_j + \sum_{k=1}^q \sum_{j=1}^p Z_{ik}X_{ij}\beta_j\gamma_{kj} + \varepsilon_i \\ &= \mathbf{Z}_i\boldsymbol{\alpha} + \mathbf{X}_i\boldsymbol{\beta} + \sum_{k=1}^q \mathbf{W}_i^{(k)}(\boldsymbol{\beta} \odot \boldsymbol{\gamma}_k) + \varepsilon_i, \end{aligned}$$

where $\boldsymbol{\alpha} = (\alpha_1, \dots, \alpha_q)'$, $\boldsymbol{\beta} = (\beta_1, \dots, \beta_p)'$, $\boldsymbol{\gamma}_k = (\gamma_{k1}, \dots, \gamma_{kp})'$, $\mathbf{W}_i^{(k)} = (Z_{ik}X_{i1}, \dots, Z_{ik}X_{ip})$, and \odot is the component-wise product. Denote \mathbf{Y} as the n -length vector composed of Y_i 's, and \mathbf{Z} , \mathbf{X} , and $\mathbf{W}^{(k)}$ as the $n \times q$, $n \times p$ and $n \times p$ design matrices composed of \mathbf{X}_i 's, \mathbf{Z}_i 's and $\mathbf{W}_i^{(k)}$'s, respectively.

For estimation and selection of important effects, consider the penalized objective function

$$Q_n(\boldsymbol{\theta}) = \frac{1}{2n} \left\| \mathbf{Y} - \mathbf{Z}\boldsymbol{\alpha} - \mathbf{X}\boldsymbol{\beta} - \sum_{k=1}^q \mathbf{W}^{(k)}(\boldsymbol{\beta} \odot \boldsymbol{\gamma}_k) \right\|_2^2 + \sum_{j=1}^p \rho(|\beta_j|; \lambda_1, r) + \sum_{j=1}^p \sum_{k=1}^q \rho(|\gamma_{kj}|; \lambda_1, r)$$

$$+ \frac{1}{2}\lambda_2\boldsymbol{\beta}'\mathbf{J}\boldsymbol{\beta} + \frac{1}{2}\lambda_2\sum_{k=1}^q\boldsymbol{\gamma}'_k\mathbf{J}\boldsymbol{\gamma}_k, \quad (2)$$

where $\boldsymbol{\theta} = (\boldsymbol{\alpha}', \boldsymbol{\beta}', \boldsymbol{\gamma}')' = (\boldsymbol{\alpha}', \boldsymbol{\beta}', \boldsymbol{\gamma}'_1, \dots, \boldsymbol{\gamma}'_q)'$, $\|\boldsymbol{\nu}\|_2$ is the L_2 norm of vector $\boldsymbol{\nu}$, $\rho(|\nu|; \lambda_1, r) = \lambda_1 \int_0^{|\nu|} \left(1 - \frac{x}{\lambda_1 r}\right)_+ dx$ is the minimax concave penalty (MCP), $\lambda_1 \geq 0$ and $\lambda_2 \geq 0$ are data-dependent tuning parameters, and $r \geq 0$ is the regularization parameter. \mathbf{J} is the $p \times p$ matrix that accommodates the structure of G measurements (more details below). The proposed estimate is defined as the minimizer of (2). The nonzero components of $\boldsymbol{\beta}$ and $\boldsymbol{\beta} \odot \boldsymbol{\gamma}_k$ ($k = 1, \dots, q$) correspond to the important main G effects and interactions that are associated with the response.

In the objective function, the first term is the lack-of-fit. Each of the first two penalty functions is the sum of p terms. For each of the G factors, penalties are imposed on its main effect as well as interactions. With the decomposition $(\beta_j \gamma_{jk})$, the proposed penalties guarantee that a G-E interaction is not identified if the corresponding main G effect is not identified. Note that here the setting and hence strategy differ from the pairwise interaction analysis studies such as Choi et al. (2010), Lim and Hastie (2015), and Hao et al. (2018). Specifically, in most G-E interaction analysis, for example as considered in our data examples, the E factors are manually selected based on extensive prior knowledge and have a low dimensionality. As such, there is no need to conduct selection with E effects, and their coefficients are always nonzero. In the literature, there are other ways of achieving the hierarchy, for example, the sparse group MCP (Liu et al., 2013). Our exploration suggests that the proposed approach has significant computational advantages.

Accommodating the structures of G measurements In (2), the underlying structures of G measurements are accommodated using the last two penalty terms. Here for interactions, instead of $\boldsymbol{\beta} \odot \boldsymbol{\gamma}_k$, we consider the structures of $\boldsymbol{\gamma}_k$ which can significantly facilitate theoretical and numerical analysis. Our numerical investigation suggests that two approaches lead to similar results (details omitted). First, consider the following two specific examples.

Consider SNP data. Assume that densely measured SNPs have been sorted according to their

physical locations on the chromosomes. Consider the following spline type penalty:

$$\sum_{j=2}^{p-1} [(\beta_{j+1} - \beta_j) - (\beta_j - \beta_{j-1})]^2 \text{ and } \sum_{j=2}^{p-1} [(\gamma_{k(j+1)} - \gamma_{kj}) - (\gamma_{kj} - \gamma_{k(j-1)})]^2. \quad (3)$$

With this penalty, we have $\mathbf{J} = \mathbf{H}'_{(p-2) \times p} \mathbf{H}_{(p-2) \times p}$ with $H_{jj} = H_{j(j+2)} = 1$, $H_{j(j+1)} = -2$, and 0 otherwise. Here \mathbf{J} is a very sparse matrix. For SNPs as well as their interactions with a specific E factor, this penalty promotes smoothness in a similar way as penalizing second order derivatives in spline-based nonparametric estimation. As a result, adjacent SNPs are promoted to have similar main effects (E-interactions) associated with the response. With main G effects, some alternatives, such as the fused lasso and smooth lasso, promote first-order smoothness, while this penalty promotes second-order smoothness. Guo et al. (2016) shows that the spline type penalty can outperform these alternatives. Another advantage of the spline type penalty is that the quadratic form is computationally more manageable than, for example, the absolute-value-based. It is noted that this study is the first to consider the spline type penalization in the context of G-E interaction analysis.

Consider gene expression data. Following published studies (Shi et al., 2015), we first construct the adjacency matrix $\mathbf{A} = (a_{jl})_{p \times p}$, where $a_{jl} = r_{jl}^{P_{corr}} I(|r_{jl}^{P_{corr}}| > c^{P_{corr}})$ with $r_{jl}^{P_{corr}}$ being the Pearson's correlation coefficient between gene expressions j and l and $c^{P_{corr}}$ being the cutoff calculated from the Fisher transformation. Note that there are multiple alternatives for constructing the adjacency matrix (Huang et al., 2011). Let $\mathbf{D} = \text{diag}(\sum_{l=1}^p |a_{1l}|, \dots, \sum_{l=1}^p |a_{pl}|)$. We consider

$$\mathbf{J} = \mathbf{I} - \mathbf{D}^{-1/2} \mathbf{A} \mathbf{D}^{-1/2}, \quad (4)$$

where \mathbf{I} is the $p \times p$ identity matrix. With the cutoff $c^{P_{corr}}$, \mathbf{J} is usually a sparse matrix. This penalty encourages the effects of correlated gene expressions to be similar, which is adjusted by the degree of adjacency. Several recent studies have established the effectiveness of this Laplacian penalization strategy for the analysis of main G effects. However, its adoption in the context of G-E interaction analysis is still lacking.

As can be seen from the above two examples, the definition of \mathbf{J} needs to be adapted to the specific data settings and may vary across data types. On the other hand, the above definitions can be extended and applied to quite a few other dense and “non-dense” cases, making the proposed analysis broadly applicable.

Accommodating other response variables In the above definition as well as some downstream developments, we use the continuous outcome and linear model as an example. The proposed approach can be extended to other data types/models. For example, in our numerical study, we consider the censored survival outcome and accelerated failure time (AFT) model. Details on this setting are provided in Appendix.

2.1 Computation

With fixed tuning parameters, optimization of (2) can be conducted using an iterative coordinate descent (CD) algorithm, which optimizes the objective function with respect to one of the three vectors, $\boldsymbol{\alpha}$, $\boldsymbol{\beta}$, and $\boldsymbol{\gamma}$, at a time and iteratively cycles through all parameters until convergence is reached. The proposed algorithm proceeds as follows:

Step 1 Initialize $t = 0$, $\boldsymbol{\beta}^{(t)} = \mathbf{0}$, $\boldsymbol{\gamma}^{(t)} = \mathbf{0}$, and $\boldsymbol{\alpha}^{(t)} = (\mathbf{Z}'\mathbf{Z})^{-1}\mathbf{Z}'\mathbf{Y}$, where $\boldsymbol{\alpha}^{(t)}$, $\boldsymbol{\beta}^{(t)}$, and $\boldsymbol{\gamma}^{(t)}$ denote the estimates of $\boldsymbol{\alpha}$, $\boldsymbol{\beta}$, and $\boldsymbol{\gamma}$ at iteration t , respectively.

Step 2 Update $t = t + 1$. With $\boldsymbol{\gamma}$ and $\boldsymbol{\alpha}$ fixed at $\boldsymbol{\gamma}^{(t-1)}$ and $\boldsymbol{\alpha}^{(t-1)}$, optimize (2) with respect to $\boldsymbol{\beta}$. Let $\tilde{\mathbf{Y}}^{(t)} = \mathbf{Y} - \mathbf{Z}\boldsymbol{\alpha}^{(t-1)}$ and $\tilde{\mathbf{X}}^{(t)} = \mathbf{X} + \sum_{k=1}^q \mathbf{W}^{(k)} \odot \left(\mathbf{1}_{n \times 1} \left(\boldsymbol{\gamma}_k^{(t-1)} \right)' \right)$ with $\mathbf{1}_{n \times 1} = (1, \dots, 1)_{n \times 1}$.

Then

$$\boldsymbol{\beta}^{(t)} = \operatorname{argmin} \frac{1}{2n} \left\| \tilde{\mathbf{Y}}^{(t)} - \tilde{\mathbf{X}}^{(t)} \boldsymbol{\beta} \right\|_2^2 + \sum_{j=1}^p \rho(|\beta_j|; \lambda_1, r) + \frac{1}{2} \lambda_2 \boldsymbol{\beta}' \mathbf{J} \boldsymbol{\beta}.$$

For $j = 1, \dots, p$, carry out the following steps sequentially.

Step 2.1 Compute

$$\operatorname{res}_{-j}^{(t)} = \tilde{\mathbf{Y}}^{(t)} - \sum_{l=1}^{j-1} \tilde{\mathbf{X}}_l^{(t)} \beta_l^{(t)} - \sum_{l=j+1}^p \tilde{\mathbf{X}}_l^{(t)} \beta_l^{(t-1)}, \quad \chi_j^{(t)} = \frac{1}{n} \left(\tilde{\mathbf{X}}_j^{(t)} \right)' \tilde{\mathbf{X}}_j^{(t)},$$

$$\varphi_j^{(t)} = \frac{1}{n} \left(\tilde{\mathbf{X}}_j^{(t)} \right)' \mathbf{res}_{-j}^{(t)}, \quad \Delta_j^{(t)} = \sum_{l=1}^{j-1} \beta_l^{(t)} J_{jl} + \sum_{l=j+1}^p \beta_l^{(t-1)} J_{jl}.$$

Step 2.2 Update the estimate of β_j as

$$\beta_j^{(t)} = \begin{cases} \frac{\text{ST}(\varphi_j^{(t)} - \lambda_2 \Delta_j^{(t)}, \lambda_1)}{\chi_j^{(t)} + \lambda_2 J_{jj} - \frac{1}{r}}, & \left| \varphi_j^{(t)} - \lambda_2 \Delta_j^{(t)} \right| \leq \lambda_1 r \left(\chi_j^{(t)} + \lambda_2 J_{jj} \right) \\ \frac{\varphi_j^{(t)} - \lambda_2 \Delta_j^{(t)}}{\chi_j^{(t)} + \lambda_2 J_{jj}}, & \left| \varphi_j^{(t)} - \lambda_2 \Delta_j^{(t)} \right| > \lambda_1 r \left(\chi_j^{(t)} + \lambda_2 J_{jj} \right) \end{cases},$$

where $\text{ST}(\nu, \lambda_1) = \text{sgn}(\nu)(|\nu| - \lambda_1)_+$ is the soft-thresholding operator.

Step 3 With β and α fixed at $\beta^{(t)}$ and $\alpha^{(t-1)}$, optimize (2) with respect to γ . Let $\check{\mathbf{Y}}^{(t)} = \mathbf{Y} - \mathbf{Z}\alpha^{(t-1)} - \mathbf{X}\beta^{(t)}$ and $(\tilde{\mathbf{W}}^{(k)})^{(t)} = \mathbf{W}^{(k)} \odot (\beta^{(t)})'$. Then

$$\left(\gamma_1^{(t)}, \dots, \gamma_q^{(t)} \right) = \underset{\gamma}{\text{argmin}} \frac{1}{2n} \left\| \check{\mathbf{Y}}^{(t)} - \sum_{k=1}^q (\tilde{\mathbf{W}}^{(k)})^{(t)} \gamma_k \right\|_2^2 + \sum_{k=1}^q \sum_{j=1}^p \rho(|\gamma_{kj}|; \lambda_1, r) + \frac{1}{2} \lambda_2 \sum_{k=1}^q \gamma_k' \mathbf{J} \gamma_k.$$

For $k = 1, \dots, q$ and $j \in \left\{ j : \beta_j^{(t)} \neq 0, j = 1, \dots, p \right\}$, conduct estimation similar to Steps 2.1 and 2.2.

Step 4 Compute $\alpha^{(t)} = (\mathbf{Z}'\mathbf{Z})^{-1} \mathbf{Z}' \left(\mathbf{Y} - \mathbf{X}\beta^{(t)} - \sum_{k=1}^q \mathbf{W}^{(k)} \left(\beta^{(t)} \odot \gamma_k^{(t)} \right) \right)$.

Step 5 Repeat Steps 2-4 until convergence. In our numerical study, convergence is concluded if $\frac{|Q_n(\boldsymbol{\theta}^{(t)}) - Q_n(\boldsymbol{\theta}^{(t-1)})|}{|Q_n(\boldsymbol{\theta}^{(t-1)})|} < 10^{-4}$.

It is noted that Steps 2 and 3 are not standard CD algorithms, which iterate until convergence. Instead, only one iteration is taken, which can significantly reduce computational cost. Details on Steps 2.1 and 2.2 are provided in Appendix. As the value of the objective function decreases at each step and is bounded below, the proposed algorithm is guaranteed to converge. Convergence is achieved in all of our numerical studies within 50 overall iterations.

Tuning parameters The proposed approach includes two tuning parameters λ_1 and λ_2 , and one regularization parameter r . For r , published studies suggest setting it as fixed or examining a small number of values. We follow the literature (Breheny and Huang, 2009) and set $r = 3$ in our numerical study. The values of (λ_1, λ_2) are chosen using BIC.

Parameter path To better comprehend the proposed penalized estimation, we simulate one replicate under the linear model with MAF setting M1 and correlation structure AR(0.3). Details on the data settings are described in Section 3. With the proposed approach, we first examine the values of BIC as a function of λ_1 and λ_2 in Figure A1. The optimal point with $(\lambda_1, \lambda_2) = (0.135, 0.095)$ is clearly identified. We further examine the parameter paths in Figure A2. The proposed approach is observed to have parameter paths similar to those of other penalized estimates. The model is sparser with larger λ_1 and smoother with larger λ_2 . For this simulated dataset, with the optimal tuning parameters, the proposed approach can correctly identify the majority of true positives while having a small number of false positives. More definitive results are presented below.

Realization To facilitate data analysis within and beyond this study, we have developed R code implementing the proposed approach and made it publicly available at www.github.com/shuanggema. The proposed approach is computationally affordable. For example, with fixed tuning parameters, for a simulated dataset with $q = 5$, $p = 5000$, and $n = 250$, the analysis can be accomplished within one minute using a laptop with standard configurations.

2.2 Statistical properties

Consider the scenario where the number of G factors increases and the number of E factors is finite as the sample size increases. This reasonably fits the analyzed datasets and others.

Let $\boldsymbol{\theta}^0 = \left((\boldsymbol{\alpha}^0)', (\boldsymbol{\beta}^0)', (\boldsymbol{\gamma}_1^0)', \dots, (\boldsymbol{\gamma}_q^0)' \right)'$ be the true parameter values, and $\boldsymbol{\Theta}^0 = \left((\boldsymbol{\alpha}^0)', (\boldsymbol{\beta}^0)', (\boldsymbol{\eta}_1^0)', \dots, (\boldsymbol{\eta}_q^0)' \right)' = \left((\boldsymbol{\alpha}^0)', (\boldsymbol{\beta}^0)', (\boldsymbol{\gamma}_1^0 \odot \boldsymbol{\beta}^0)', \dots, (\boldsymbol{\gamma}_q^0 \odot \boldsymbol{\beta}^0)' \right)'$. Let $\mathcal{A}_1 = \{j : \beta_j^0 \neq 0\}$, $\mathcal{A}_2^k = \{j : \gamma_{kj}^0 \neq 0 \text{ and } \beta_j^0 \neq 0\}$, and $\mathcal{A}_2 = \mathcal{A}_2^1 \cup \dots \cup \mathcal{A}_2^q$. Note that all α_k^0 's are nonzero, and the corresponding parameters are not subject to penalization in estimation. With the hierarchical constraint, in \mathcal{A}_2^k , we are only interested in nonzero γ_{kj} 's for which the corresponding β_j 's are also nonzero. Here, we have $j \in \mathcal{A}_1$ if for some k , $j \in \mathcal{A}_2^k$. Denote $|\mathcal{A}|$ as the cardinality of set \mathcal{A} . Let $s = |\mathcal{A}_1| + |\mathcal{A}_2^1| + \dots + |\mathcal{A}_2^q|$. For a vector $\boldsymbol{\nu}$ and index set \mathcal{S} , let $\boldsymbol{\nu}_{\mathcal{S}}$ denote the components of $\boldsymbol{\nu}$ indexed by \mathcal{S} . For a matrix \boldsymbol{M} and two index sets \mathcal{S}_1 and \mathcal{S}_2 , denote $\boldsymbol{M}_{\mathcal{S}_1}$ and

$M_{\mathcal{S}_1}$. as the columns and rows of M indexed by \mathcal{S}_1 , and $M_{\mathcal{S}_1, \mathcal{S}_2}$ as the submatrix of M indexed by \mathcal{S}_1 and \mathcal{S}_2 .

Denote $\boldsymbol{\theta}_{\mathcal{A}}^* = \left((\boldsymbol{\alpha}^*)', (\boldsymbol{\beta}_{\mathcal{A}_1}^*)', (\boldsymbol{\gamma}_{1, \mathcal{A}_2^1}^*)', \dots, (\boldsymbol{\gamma}_{q, \mathcal{A}_2^q}^*)' \right)'$ as the minimizer of

$$\begin{aligned} \tilde{Q}_n(\boldsymbol{\theta}_{\mathcal{A}}) &= \frac{1}{2n} \left\| \mathbf{Y} - \mathbf{Z}\boldsymbol{\alpha} - \mathbf{X}_{\mathcal{A}_1}\boldsymbol{\beta}_{\mathcal{A}_1} - \sum_{k=1}^q \mathbf{W}_{\mathcal{A}_2^k}^{(k)} \left(\boldsymbol{\beta}_{\mathcal{A}_2^k} \odot \boldsymbol{\gamma}_{k, \mathcal{A}_2^k} \right) \right\|_2^2 \\ &\quad + \frac{1}{2} \lambda_2 \left(\boldsymbol{\beta}'_{\mathcal{A}_1} \mathbf{J}_{\mathcal{A}_1, \mathcal{A}_1} \boldsymbol{\beta}_{\mathcal{A}_1} + \sum_{k=1}^q \boldsymbol{\gamma}'_{k, \mathcal{A}_2^k} \mathbf{J}_{\mathcal{A}_2^k, \mathcal{A}_2^k} \boldsymbol{\gamma}_{k, \mathcal{A}_2^k} \right). \end{aligned}$$

The following conditions are assumed:

(C1) Components of the residual $\boldsymbol{\varepsilon}$ are i.i.d and sub-Gaussian with noise level σ . That is, for any vector $\boldsymbol{\nu}$ with $\|\boldsymbol{\nu}\|_2 = 1$ and any constant $\epsilon > 0$, $P(|\boldsymbol{\nu}'\boldsymbol{\varepsilon}| \geq \epsilon) \leq 2 \exp\left(-\frac{\epsilon^2}{2\sigma^2}\right)$.

(C2) Let $b_0 = \min\left\{\left\{|\beta_j^0| : j \in \mathcal{A}_1\right\}, \left\{|\gamma_{kj}^0| : j \in \mathcal{A}_2^k, k = 1, \dots, q\right\}\right\}$. Then, $b_0\sqrt{n/s} \rightarrow \infty$.

(C3) Use $\lambda_{\min}(\mathbf{M})$ and $\lambda_{\max}(\mathbf{M})$ to denote the smallest and largest eigenvalues of matrix \mathbf{M} .

Then,

$$\max_{\boldsymbol{\theta}_{\mathcal{A}} \in \mathcal{N}_0} \lambda_{\max} \left(\frac{1}{n} \mathbf{G}(\boldsymbol{\beta}_{\mathcal{A}_2}, \boldsymbol{\gamma}_{\mathcal{A}_1})' \mathbf{G}(\boldsymbol{\beta}_{\mathcal{A}_2}, \boldsymbol{\gamma}_{\mathcal{A}_1}) \right) \leq s\bar{c},$$

and

$$\min_{\boldsymbol{\theta}_{\mathcal{A}} \in \mathcal{N}_0} \lambda_{\min} \left(\frac{1}{n} \mathbf{G}(\boldsymbol{\beta}_{\mathcal{A}_2}, \boldsymbol{\gamma}_{\mathcal{A}_1})' \mathbf{G}(\boldsymbol{\beta}_{\mathcal{A}_2}, \boldsymbol{\gamma}_{\mathcal{A}_1}) + \frac{1}{n} \mathbf{F}(\boldsymbol{\theta}_{\mathcal{A}}) \right) \geq \underline{c},$$

where $\boldsymbol{\gamma}_{\mathcal{A}_1} = \left(\boldsymbol{\gamma}'_{1, \mathcal{A}_1}, \dots, \boldsymbol{\gamma}'_{q, \mathcal{A}_1} \right)'$ with $\gamma_{kj} = 0$, if $j \in \mathcal{A}_1$ but $j \notin \mathcal{A}_2^k$,

$$\mathbf{G}(\boldsymbol{\beta}_{\mathcal{A}_2}, \boldsymbol{\gamma}_{\mathcal{A}_1}) = \left(\mathbf{Z}, \mathbf{U}(\boldsymbol{\gamma}_{\mathcal{A}_1}), \mathbf{V}^{(1)}(\boldsymbol{\beta}_{\mathcal{A}_2^1}), \mathbf{V}^{(2)}(\boldsymbol{\beta}_{\mathcal{A}_2^2}), \dots, \mathbf{V}^{(q)}(\boldsymbol{\beta}_{\mathcal{A}_2^q}) \right)_{n \times (q+s)},$$

with

$$\mathbf{U}(\boldsymbol{\gamma}_{\mathcal{A}_1}) = \mathbf{X}_{\mathcal{A}_1} + \sum_{k=1}^q \mathbf{W}_{\mathcal{A}_1}^{(k)} \odot (\mathbf{1}_{n \times 1} (\boldsymbol{\gamma}_{k, \mathcal{A}_1})'), \quad \mathbf{V}^{(k)}(\boldsymbol{\beta}_{\mathcal{A}_2^k}) = \mathbf{W}_{\mathcal{A}_2^k}^{(k)} \odot \left(\mathbf{1}_{n \times 1} (\boldsymbol{\beta}_{\mathcal{A}_2^k})' \right),$$

$\mathbf{F}(\boldsymbol{\theta}_{\mathcal{A}}) = (f_{jl}(\boldsymbol{\theta}_{\mathcal{A}}))_{(q+s) \times (q+s)}$ with $f_{jl}(\boldsymbol{\theta}_{\mathcal{A}}) = -\left(\mathbf{W}_{\zeta}^{(k)}\right)' (\mathbf{Y} - \mathbf{Z}\boldsymbol{\alpha} - \mathbf{X}_{\mathcal{A}_1}\boldsymbol{\beta}_{\mathcal{A}_1} - \sum_{g=1}^q \mathbf{W}_{\mathcal{A}_2^g}^{(g)}(\boldsymbol{\beta}_{\mathcal{A}_2^g} \odot \boldsymbol{\gamma}_{g, \mathcal{A}_2^g}))$ if both j and l correspond to the ζ th element of \mathcal{A}_2^k , and 0 otherwise, $\mathcal{N}_0 = \{\boldsymbol{\theta}_{\mathcal{A}} : \|\boldsymbol{\theta}_{\mathcal{A}} - \boldsymbol{\theta}_{\mathcal{A}}^0\|_{\infty} \leq \frac{b_0}{2}\}$, and \bar{c} and \underline{c} are two positive constants.

(C4) $\lambda_2 = O(\sqrt{1/n})$.

(C5) $\lambda_{\min}(\tilde{\mathbf{J}}_{\mathcal{A},\mathcal{A}}) \geq 0$ and $\|\tilde{\mathbf{J}}_{\mathcal{A},\mathcal{A}}\boldsymbol{\theta}_{\mathcal{A}}^0\|_2 = O(\sqrt{s})$, where $\tilde{\mathbf{J}}_{\mathcal{A},\mathcal{A}} = \text{diag}(\mathbf{0}_{q \times q}, \mathbf{J}_{\mathcal{A}_1, \mathcal{A}_1}, \dots, \mathbf{J}_{\mathcal{A}_2^q, \mathcal{A}_2^q})$ is a block diagonal matrix with the diagonal blocks being $\mathbf{0}_{q \times q}$, $\mathbf{J}_{\mathcal{A}_1, \mathcal{A}_1}$, \dots , and $\mathbf{J}_{\mathcal{A}_2^q, \mathcal{A}_2^q}$.

Condition (C1) is the sub-Gaussian condition which is commonly assumed in published studies (Fan and Lv, 2011; Guo et al., 2016; Huang et al., 2017). Condition (C2) puts a lower bound on the size of the smallest signal. Condition (C3) assumes that the predictor matrix is “well behaved”. Similar conditions have been assumed in Zou and Zhang (2009), Fan and Lv (2011), and others. Condition (C4) restricts the rate of the tuning parameter λ_2 . Condition (C5) makes a weak constraint on \mathbf{J} . It needs to be checked on a case-by-case basis, as \mathbf{J} may vary across data. For the spline type penalty considered for SNP data, Condition (C5) is easily satisfied. For the Laplacian type penalty, it is also satisfied for example when the network is sparse.

Theorem 1: Under Conditions (C1)-(C5), there exists a local minimizer $\boldsymbol{\theta}_{\mathcal{A}}^*$ of $\tilde{Q}_n(\boldsymbol{\theta}_{\mathcal{A}})$ such that for any constant $E > 0$,

$$P\{\|\boldsymbol{\theta}_{\mathcal{A}}^* - \boldsymbol{\theta}_{\mathcal{A}}^0\|_2 \leq \delta_n\} > 1 - \xi,$$

$$\text{where } \delta_n = \frac{4\lambda_2\|\tilde{\mathbf{J}}_{\mathcal{A},\mathcal{A}}\boldsymbol{\theta}_{\mathcal{A}}^0\|_2}{\underline{c}} + E\sqrt{s/n} \text{ and } \xi = \exp\left(-\frac{[4\sqrt{n/s}\lambda_2\|\tilde{\mathbf{J}}_{\mathcal{A},\mathcal{A}}\boldsymbol{\theta}_{\mathcal{A}}^0\|_2 + E\underline{c}]^2}{32\sigma^2\bar{c}}\right).$$

Proof is provided in Appendix. With Theorem 1, we have

$$\|\boldsymbol{\theta}_{\mathcal{A}}^* - \boldsymbol{\theta}_{\mathcal{A}}^0\|_2 = O_p(\sqrt{s/n}) \text{ and } \|\boldsymbol{\Theta}_{\mathcal{A}}^* - \boldsymbol{\Theta}_{\mathcal{A}}^0\|_2 = O_p(\sqrt{s/n}),$$

as $\lambda_2 = O(\sqrt{1/n})$ and $\|\tilde{\mathbf{J}}_{\mathcal{A},\mathcal{A}}\boldsymbol{\theta}_{\mathcal{A}}^0\|_2 = O(\sqrt{s})$. This theorem establishes estimation consistency when the true sparsity structure is known.

Let $\mathcal{A}_1^c = \{j : \beta_j^0 = 0\}$ and $(\tilde{\mathcal{A}}_2^k)^c = \{j : \gamma_{kj}^0 = 0 \text{ and } \beta_j^0 \neq 0\}$. Then we have $(\tilde{\mathcal{A}}_2^k)^c \cup \mathcal{A}_1^c = \{j : \eta_{kj}^0 = 0\}$. The following additional conditions are assumed.

$$\begin{aligned} \text{(C6)} \quad & \|\mathbf{U}(\boldsymbol{\gamma}_{\mathcal{A}_1^c}^0)' \mathbf{G}(\boldsymbol{\beta}_{\mathcal{A}_2}^0, \boldsymbol{\gamma}_{\mathcal{A}_1}^0)\|_{2,\infty} = O(n), \left\| \mathbf{V}^{(k)} \left(\boldsymbol{\beta}_{(\tilde{\mathcal{A}}_2^k)^c}^0 \right)' \mathbf{G}(\boldsymbol{\beta}_{\mathcal{A}_2}^0, \boldsymbol{\gamma}_{\mathcal{A}_1}^0) \right\|_{2,\infty} = O(n), \\ & \|\mathbf{U}(\boldsymbol{\gamma}_j^0)\|_2 = O(\sqrt{n}), \|\mathbf{V}^{(k)}(\beta_j^0)\|_2 = O(\sqrt{n}), j = 1, \dots, p, \end{aligned}$$

where for matrix \mathbf{M} , $\|\mathbf{M}\|_{2,\infty} = \max_{\|\boldsymbol{\nu}\|_2=1} \|\mathbf{M}\boldsymbol{\nu}\|_\infty$, and $\mathbf{U}(\cdot)$ and $\mathbf{V}^{(k)}(\cdot)$ are defined in Condition (C3).

$$\max_{\boldsymbol{\theta}_{\mathcal{A}} \in \mathcal{N}_0} \max_j \lambda_{\max} \left(\mathbf{T}_1^{(j)}(\boldsymbol{\gamma}_j) \right) = O(n),$$

where $\mathbf{T}_1^{(j)}(\boldsymbol{\gamma}_j) = \left(t_{lh}^{(j)}(\boldsymbol{\gamma}_j) \right)_{(q+s) \times (q+s)}$ with $t_{lh}^{(j)}(\boldsymbol{\gamma}_j) = \left(\mathbf{X}_j + \sum_{g=1}^q \mathbf{W}_j^{(g)} \boldsymbol{\gamma}_{gj} \right)' \mathbf{W}_\varsigma^{(k)}$ if both l and h correspond to the ς th element of \mathcal{A}_2^k , and 0 otherwise.

$$\max_{\boldsymbol{\theta}_{\mathcal{A}} \in \mathcal{N}_0} \max_j \lambda_{\max} \left(\mathbf{T}_2^{(j)}(\boldsymbol{\beta}_j) \right) = O(n),$$

where $\mathbf{T}_2^{(j)}(\boldsymbol{\beta}_j) = \left(t_{lh}^{(j)}(\boldsymbol{\beta}_j) \right)_{(q+s) \times (q+s)}$ with $t_{lh}^{(j)}(\boldsymbol{\beta}_j) = \left(\mathbf{W}_j^{(k)} \boldsymbol{\beta}_j \right)' \mathbf{W}_\varsigma^{(k)}$ if both l and h correspond to the ς th element of \mathcal{A}_2^k , and 0 otherwise.

$$(C7) \quad \log(p) = n^a, a \in (0, \frac{1}{2}).$$

$$(C8) \quad \frac{\lambda_1}{\sqrt{s/n}} \rightarrow \infty, \quad \frac{\lambda_1}{n^{a/2-1/2} \sqrt{\log n}} \rightarrow \infty.$$

$$(C9) \quad b_0 \lambda_1^{-1} \rightarrow \infty.$$

Condition (C6) is similar to Condition 4 in Fan and Lv (2011), where the first two equations control the ‘‘correlations’’ between the unimportant and important variables. Condition (C7) allows the number of G factors to increase as the sample size increases. Condition (C8) has also been assumed in Fan and Lv (2011) and others. Condition (C9) provides the rate at which the nonzero coefficients can be distinguished from zero (Huang et al., 2017).

Theorem 2: Define $\hat{\boldsymbol{\theta}}$ as $\hat{\boldsymbol{\theta}}_{\mathcal{A}} = \boldsymbol{\theta}_{\mathcal{A}}^*$, $\hat{\boldsymbol{\beta}}_{\mathcal{A}_1^c} = 0$, $\hat{\boldsymbol{\gamma}}_{k,(\bar{\mathcal{A}}_2^k)^c} = 0$ and $\hat{\boldsymbol{\gamma}}_{k,\mathcal{A}_1^c}$ being the minimizer of $Q_n(\boldsymbol{\theta})$ with other parameters fixed at the values defined as above. Then under Conditions (C1)-(C9), with probability tending to 1, $\hat{\boldsymbol{\theta}}$ is a strict local minimizer of $Q_n(\boldsymbol{\theta})$.

Proof is provided in Appendix. With Theorem 2, we have $\hat{\boldsymbol{\eta}}_{k,\mathcal{A}_1^c} = 0$ with $\hat{\boldsymbol{\beta}}_{\mathcal{A}_1^c} = 0$, and $\hat{\boldsymbol{\eta}}_{k,(\bar{\mathcal{A}}_2^k)^c} = 0$ with $\hat{\boldsymbol{\gamma}}_{k,(\bar{\mathcal{A}}_2^k)^c} = 0$. Theorem 2 establishes the selection and estimation consistency properties of the proposed approach under high-dimensional settings.

3 Simulation

We simulate densely positioned SNP data, which have an adjacency structure. Specifically, (a) under all scenarios, $q = 5$ and $p = 5,000$. Thus, there are a total of 5,005 main effects and 25,000 interactions. (b) Two approaches, A1 and A2, are adopted to simulate G factors which mimic SNP data coded with three categories (0, 1, 2) for genotypes (aa, Aa, AA). (c) The A1 approach includes two steps, under which we first generate p continuous variables from a multivariate Normal distribution with mean $\mathbf{0}$ and covariance matrix $\Sigma = (\sigma_{jl})_{p \times p}$, and then dichotomize the continuous variables at q_1 and q_2 quantiles to generate 3-level G measurements (0, 1, 2). In the first step, two correlation structures are considered with different parameters. The first is the auto-regressive (AR) structure with $\sigma_{jl} = \rho^{|j-l|}$. We consider two levels of correlation with $\rho = 0.3$ and 0.5 . The second is the banded correlation structure where two specific scenarios are considered. The first one (Band1) has $\sigma_{jl} = 1$ if $j = l$, 0.3 if $|j-l| = 1$, and 0 otherwise. The second one (Band2) has $\sigma_{jl} = 1$ if $j = l$, 0.5 if $|j-l| = 1$, 0.3 if $|j-l| = 2$, and 0 otherwise. In the second step, the quantiles q_1 and q_2 are adjusted to generate G factors with different minor allele frequency (MAF) values. Consider two specific scenarios. Under the first scenario (M1), all of the G factors have MAF=0.05 with $q_1 = 0.91$ and $q_2 = 0.99$. Under the second one (M2), a half of the G factors have MAF=0.05, and the other half have MAF=0.15 with $q_1 = 0.73$ and $q_2 = 0.97$. (d) Under the A2 approach, we simulate G factors with the pairwise LD structure. Specifically, denote p_A and p_B as the MAFs of alleles A and B for two adjacent SNPs. The LD is defined as $\phi = r_{LD} \sqrt{p_A(1-p_A)p_B(1-p_B)}$ with pairwise correlation r_{LD} . Then, the four haplotypes ab, aB, Ab, AB have frequencies $(1-p_A)(1-p_B) + \phi$, $(1-p_A)p_B - \phi$, $p_A(1-p_B) - \phi$, and $p_A p_B + \phi$, respectively. Following the literature (Wu et al., 2015), with the Hardy-Weinberg equilibrium assumption, we simulate the SNP genotype (AA, Aa, aa) at locus 1 from a multinomial distribution given corresponding frequencies $(p_A^2, 2p_A^2(1-p_A), (1-p_A)^2)$ and that at locus 2 accordingly from the conditional probability defined in Cui et al. (2008). Two pairwise correlations are considered with $r_{LD} = 0.3$ and $r_{LD} = 0.5$. For MAF, two scenarios similar to those

in Step 2 of A1 are considered. (e) For E factors, we first generate five continuous variables from a multivariate Normal distribution with marginal mean 0, marginal variance 1, and AR correlation ($\rho = 0.3$), and then dichotomize two of them at 0 and create two binary variables. There are thus three continuous and two binary E factors. (f) For E factors, their coefficients $\alpha_k, k = 1, \dots, 5$ are generated from Uniform (0.8, 1.2). There are 20 main G effects and 40 G-E interactions with nonzero coefficients. Two structures, the “main effects, interactions” hierarchical structure and the smoothness structure of SNP effects, are satisfied. Specifically, we set $\beta_j = \sin(0.2j + 0.9) + 0.2$ for $j = 1, \dots, 10$, $\beta_j = 0.5(j - 10)$ for $j = 11, \dots, 15$, $\beta_j = 0.5(21 - j)$ for $j = 16, \dots, 20$, $\eta_{1j} = 0.2j + 0.2$ for $j = 1, \dots, 5$, $\eta_{1j} = 0.2(11 - j) + 0.2$ for $j = 6, \dots, 11$, $\eta_{2j} = 0.2\sqrt{3j - 32}$ for $j = 11, \dots, 15$, $\eta_{2j} = 0.2\sqrt{63 - 3j}$ for $j = 16, \dots, 20$, $\eta_{3j} = -(0.2j - 0.9)^2 + 1.5$ for $j = 1, \dots, 10$, and $\eta_{3j} = -(0.2j - 3.2)^2 + 1.6$ for $j = 11, \dots, 20$. The rest of the effects are zero. A graphical presentation is provided in Figure 1, where the sparsity and smoothness of effects are easy to see. (g) Consider two types of response variables and models. The first is a continuous response under model (1). The second is a censored survival response under the AFT model, where the censoring times are generated from an exponential distribution with parameter adjusted to achieve $\sim 20\%$ censoring. For both models, the random error ε_i follows a standard Normal distribution. (h) Set the sample size $n = 250$ and $n = 350$ for the continuous and survival settings, respectively. There are a total of 24 scenarios, comprehensively covering a wide spectrum with different types of responses and correlation structures among G factors, and various levels of MAF.

For the simulated data, we consider the proposed approach with the spline type penalty defined in (3). We also consider the following alternatives. **MA**, which is a marginal analysis approach that analyzes one G factor along with all E factors and corresponding interactions at a time. P-values of the G factors and interactions are adjusted using the false discovery rate (FDR) approach. This approach has been commonly adopted in published studies and is a suitable benchmark for comparison. **HierMCP**, which is the non-structured counterpart of the proposed approach, where

the MCP penalty is applied for estimation and selection. Comparing with this approach can reveal the value of incorporating the two structures. **SMCP**, which is based on model (1) and imposes the MCP and structured penalties on β_j and η_{kj} without respecting the “main effects, interactions” hierarchy. Comparing with this approach can reveal the value of the special consideration on interactions. We acknowledge that there are other interaction analysis approaches that can be applied to the simulated data. The above alternatives are adopted as they are perhaps the most relevant. Comparing with them can in a relatively direct way establish the merit of the proposed structured penalization and decomposition strategy for interaction analysis.

When evaluating identification performance, both main effects and interactions are considered. Measures used include the number of true positives (M:TP) and false positives (M:FP) for main effects, and number of true positives (I:TP) and false positives (I:FP) for interactions. Estimation performance is assessed using the root sum of squared errors (RSSE) defined as $\|\hat{\Theta} - \Theta^0\|_2$, where $\hat{\Theta}$ and Θ^0 are the estimated and true values of $\Theta = (\alpha', \beta', \eta'_1, \dots, \eta'_q)'$. We also take the underlying structure of SNPs into consideration and compute the root structured error (RSE) $\sqrt{(\hat{\Theta} - \Theta^0)' \tilde{\mathbf{J}} (\hat{\Theta} - \Theta^0)}$, where $\tilde{\mathbf{J}} = \text{diag}(\mathbf{0}_{q \times q}, \mathbf{J}, \dots, \mathbf{J})$. For evaluating prediction performance, an independent testing set with 100 subjects is generated for each simulated dataset. We adopt the prediction mean squared error (PMSE) for continuous outcomes and C-statistic (Cstat) for censored survival outcomes. C-statistic is the time-integrated area under the time-dependent ROC framework and measures the overall adequacy of risk prediction for censored survival data, with a larger value indicating better prediction.

For each scenario, 500 replicates are simulated, and the means and standard deviations (sd) of the evaluation measures are computed. Summary results under the linear model with MAF settings M1 and M2 are shown in Tables 1 and 2, respectively. The rest of the results are shown in Appendix. Across all simulation scenarios, the proposed approach is observed to have superior or similar performance compared to the alternatives. Specifically, it can more accurately identify both

the true main effects and interactions while having a small number of false positives. For example in Table 1 with AR(0.3), the proposed approach has (M:TP,M:FP,I:TP,I:FP)=(19.7,0.0,33.8,4.1), compared to (0.1,11.2,2.2,77.9) for MA, (11.7,68.5,3.4,4.2) for HierMCP, and (17.4,2.7,23.4,19.7) for SMCP. Compared to MA and HierMCP, the proposed approach has much better identification performance, which provides a strong support to the structured analysis strategy. It also outperforms SMCP, which suggests the effectiveness of the proposed decomposition strategy for respecting the interaction hierarchy. The advantage of the proposed approach gets more prominent under MAF setting M2. For example in Table 2 with Band1, the proposed approach has (M:TP,M:FP,I:TP,I:FP)=(19.7,1.0,33.3,5.1), compared to (0.1,6.7,1.6,53.6) for MA, (11.7,64.7,3.9,5.2) for HierMCP, and (16.1,7.0,11.3,74.1) for SMCP. We also observe the superiority of the proposed approach in estimation. For example in Table 1 with LD(0.5), the proposed approach has RSSE=2.95, compared to 16.15 (MA), 17.76 (HierMCP), and 4.93 (SMCP). It also has smaller structured errors. In addition, the proposed approach has satisfactory prediction performance. For example in Table 2 with Band2, the PMSEs are 29.94 (MA), 23.04 (HierMCP), 4.18 (SMCP), and 1.59 (proposed). The observed patterns for data with survival outcomes (Tables A1 and A2) are similar, where the proposed approach performs better than or comparable to the alternatives.

For SNP data, we have also examined a few other simulation scenarios, and the observed patterns are similar (details omitted). We have also experimented with continuously distributed G measurements, which mimic gene expression data, and applied the Laplacian type penalty function. Similar superiority of the proposed approach is observed (details omitted).

4 Data analysis

4.1 GENEVA diabetes data (NHS/HPFS)

The Gene Environment Association Studies (GENEVA) consortium is part of the Genes, Environment and Health Initiative (GEI) organized by the NIH. We analyze the GENEVA Type 2

Diabetes data, where the goal is to identify genetic factors that are associated with type 2 diabetes phenotypes, biomarkers, and others. In our analysis, data are downloaded from dbGaP (accession number phs000091.v2.p1). The response variable of interest is body mass index (BMI), which is continuously distributed. BMI level is one of the most important risk factors for type 2 diabetes. Following recent published studies, we take a “loose” definition of E factors. Specifically, E factors considered include age, family history of diabetes among first degree relatives (famdb), total physical activity (act), trans fat intake (trans), cereal fiber intake (ceraf), and heme iron intake (heme), all of which have been suggested to be potentially associated with BMI and diabetes. For G factors, we analyze SNPs on chromosome 4, which plays an important role in many disorders, such as Parkinson’s disease, Huntington’s disease, and others. Preprocessing similar to that in Wu et al. (2014) is conducted, which includes subject matching, standard quality control for SNPs, and missing data imputation. Data are available on 2,558 subjects and 40,568 SNPs. As the number of relevant SNPs is not expected to be large, to improve stability, we conduct a marginal screening. Specifically, a p-value is computed for each SNP based on a marginal linear model. Then the region of 10,000 consecutive SNPs with the smallest sum of p-values is selected for downstream analysis. With the physical adjacency structure in mind, in the prescreening, we select a region (as opposed to individual SNPs).

We adopt the linear regression model and spline type penalty (3). The proposed approach identifies 71 main SNP effects and 128 G-E interactions. The detailed estimation results are provided in Table 3 and also presented in Figure A3, where SNPs are sorted according to their physical locations on the chromosome. In terms of main effects, three E factors, age, act, and ceraf, have negative coefficients, and the other three, famdb, trans, and heme, have positive coefficients, which are consistent with findings in the literature. Figure A3 shows that the estimated effects demonstrate a certain degree of smoothness, which fits the design of the proposed approach. Genes that the identified SNPs belong to or are the closest to are also provided in Table 3. Literature search

suggests that these genes and interactions may have important implications, which may provide support to the validity of the proposed approach. For example, gene NPPFR2 has been found to play an important role in obesity predisposition, and some NPPFR2 haplotypes have been suggested to be strongly protective against obesity. Gene CXCL2 has been shown to be up-regulated in obese subjects and contribute to the chemotaxis of neutrophils which are one type of circulating cells greatly activated in obese subjects. Published analysis has also found that the enzyme encoded by gene GK2 plays a key role in the regulation of glycerol uptake and metabolism, and its activity in human adipose tissue is related to obesity.

Beyond the proposed approach, we also conduct analysis using the alternatives. The summary comparison results are shown in Table A3. It is observed that the proposed approach identifies different main G effects and more significantly different interactions from those with the alternatives. Without reinforcing the interaction hierarchical structure, SMCP identifies the smallest number of main effects but the second largest number of interactions. Both the proposed approach and HierMCP identify a moderate number of main effects and interactions.

With real data, it is difficult to objectively evaluate identification accuracy. To provide support to the identification results, we examine prediction performance and selection stability using a resampling-based approach (Huang and Ma, 2010). With 500 resamplings, we compute the mean PMSEs, which are 15.38 (MA), 17.47 (HierMCP), 13.11 (SMCP), and 13.06 (proposed). The proposed approach has prediction performance comparable to SMCP and better than MA and HierMCP. We further compute the observed occurrence index (OOI) to measure selection stability. It is the probability of a specific main effect or interaction identified in 500 resamplings. The mean OOI values for the identified main G effects and interactions using the proposed approach is 0.69, compared to 0.47 (MA), 0.39 (HierMCP), and 0.21 (SMCP). The proposed approach has a prominent superiority in selection stability.

4.2 TCGA skin cutaneous melanoma data

We consider The Cancer Genome Atlas (TCGA) skin cutaneous melanoma (SKCM) data. TCGA is a collective effort organized by NIH and has published high quality clinical, environmental, and genetic data. We focus on the processed level 3 data, which are downloaded from TCGA Provisional using the R package *cgdsr*. As in several recent published studies, we analyze the (censored) overall survival. The analyzed E factors include age, AJCC nodes pathologic stage (PN), gender, Breslow’s depth, and Clark level, all of which have been extensively studied in the literature. For G factors, we consider the mRNA gene expressions. In TCGA, gene expression measurements are the z-scores, which have been lowess-normalized, log-transformed and median-centered, and quantify the relative expressions of tumor samples with respect to normal. Data are available on 298 subjects and 18,934 gene expressions. Among the subjects, 152 died during followup. Marginal screening is also conducted, and the 10,000 genes with the smallest p-values are selected for downstream analysis. Here as genes can be physically far from each other, the screening is directly based on p-values to select individual genes.

With a censored survival outcome, we adopt the AFT model. Examining the estimation procedure described in Appendix suggests that the proposed computational algorithm can be directly applied. With gene expression measurements, we adopt the Laplacian type penalty (4). The proposed analysis identifies 50 main G effects and 44 interactions. The detailed estimation results are provided in Table 4. All five E factors except for gender have negative coefficients, which match observations in the literature. The identified genes are also presented in Figure A4, where two genes are connected if they have a nonzero adjacency value. For the identified genes, published studies provide independent evidences of their associations with cutaneous melanoma. For example, ACTL6A (BAF53) is a subunit of the SWI/SNF complex which has been found to be critical for the expression of microphthalmia-associated transcription factor in melanoma cells. FAM131B-BRAF fusion has been observed to comprise an alternative mechanism of MAPK pathway activation,

and MAPK pathway plays important roles in melanoma etiology, prognosis, and treatment. Gene GOLPH3 has been shown to regulate cell size and enhance growth-factor-induced mTOR signaling in melanoma cells, and suggested as a new oncogene that is commonly targeted for amplification in melanoma. Gene IL17A has been found to have tumorigenic effects in melanoma cell lines, which are related to the signal transducer and activator of transcription pathway signaling. It has been demonstrated that mutations in RAC1 are potentially biologically associated with cutaneous melanoma, and the pharmacological inhibition of downstream effectors of RAC1 signaling could be of therapeutic benefit. In addition, gene SERPINB3 has been reported to be up-regulated in benign hyperplasia in melanoma.

Analysis is further conducted using the three alternatives, and the summary comparison results are presented in Table A3. As for the previous dataset, the proposed approach identifies different sets of main effects and interactions. We also evaluate prediction performance and selection stability. In prediction evaluation, the mean C-statistics over 500 resamplings are 0.54 (MA), 0.59 (HierMCP), 0.64 (SMCP), and 0.65 (Proposed). In addition, the average OOI of the proposed approach is 0.87, compared to 0.53 (MA), 0.55 (HierMCP), and 0.77 (SMCP). The proposed approach again has better prediction performance and stability.

5 Discussion

For G-E interaction analysis, in this article, we have developed a new approach which shares similar desirable properties as the existing ones but also advances from them by accommodating the underlying structures of G factors. Although structured analysis has been conducted for main G effects in some recent publications, this study is among the first to conduct structured analysis in the context of G-E interaction analysis. Significant complexity is brought by the multiple effects (coefficients) that correspond to one G factor and the need to respect the “main effects, interactions” hierarchy. The proposed approach belongs to the well-established penalization paradigm and has an

intuitive definition. Although it has multiple penalty terms, it is computationally much manageable. It is proved to have the consistency properties, which have not been established for most alternatives and provide a uniquely strong ground for the proposed approach. Extensive numerical studies show the practical superiority. Overall, this study provides a practically useful new way for analyzing G-E interactions.

Although described using the linear regression model for a continuous response as an example, the proposed approach can be extended to other data settings/models. It can accommodate multiple types of structures, as long as the \mathbf{J} matrix satisfies certain mild conditions. As shown in published studies, \mathbf{J} may need to be defined on a case-by-case basis. We leave it to future research to study the definition and properties of \mathbf{J} for other types of omics data.

Acknowledgments

This work was partly supported by the National Institutes of Health [CA216017, CA204120]; National Natural Science Foundation of China [61402276, 91546202]; and Bureau of Statistics of China [2016LD01, 2018LD02].

References

- Barabasi, A., Gulbahce, N., & Loscalzo, J. (2011). Network medicine: a network-based approach to human disease. *Nature Reviews Genetics*, 12(1), 56-68.
- Bien, J., Taylor, J., & Tibshirani, R. (2013). A lasso for hierarchical interactions. *Annals of Statistics*, 41(3), 1111-1141.
- Breheny, P., & Huang, J. (2009). Penalized methods for bi-level variable selection. *Statistics and its Interface*, 2(3), 369-380.
- Choi, N. H., Li, W., & Zhu, J. (2010). Variable selection with the strong heredity constraint and its oracle property. *Journal of the American Statistical Association*, 105(489), 354-364.
- Cui, Y., Kang, G., Sun, K., Qian, M., Romero, R., & Fu, W. (2008). Gene-centric genomewide association study via entropy. *Genetics*, 179(1), 637-650.
- Fan, J., & Lv, J. (2011). Nonconcave penalized likelihood with NP-dimensionality. *IEEE Transactions on Information Theory*, 57(8), 5467-5484.
- Guo, J., Hu, J., Jing, B. Y., & Zhang, Z. (2016). Spline-lasso in high-dimensional linear regression. *Journal of the American Statistical Association*, 111(513), 288-297.
- Hao, N., & Zhang, H. H. (2017). A note on high dimensional linear regression with interactions. *American Statistician*, 71(4), 291-297.

- Hao, N., Feng, Y., & Zhang, H. H. (2018). Model selection for high dimensional quadratic regression via regularization. *Journal of the American Statistical Association*, 113, 615-625.
- Hebiri, M., & van de Geer, S. (2011). The Smooth-Lasso and other $l_1 + l_2$ -penalized methods. *Electronic Journal of Statistics*, 5, 1184-1226.
- Huang, J., & Ma, S. (2010). Variable selection in the accelerated failure time model via the bridge method. *Lifetime Data Analysis*, 16(2), 176-195.
- Huang, J., Ma, S., Li, H., & Zhang, C. H. (2011). The sparse Laplacian shrinkage estimator for high-dimensional regression. *Annals of Statistics*, 39(4), 2021-2046.
- Huang, Y., Zhang, Q., Zhang, S., Huang, J., & Ma, S. (2017). Promoting similarity of sparsity structures in integrative analysis with penalization. *Journal of the American Statistical Association*, 112(517), 342-350.
- Kim, S., Pan, W., & Shen, X. (2013). Network-based penalized regression with application to genomic data. *Biometrics*, 69(3), 582-593.
- Li, C., & Li, H. (2008). Network-constrained regularization and variable selection for analysis of genomic data. *Bioinformatics*, 24(9), 1175-1182.
- Li, C., & Li, H. (2010). Variable selection and regression analysis for graph-structured covariates with an application to genomics. *The Annals of Applied Statistics*, 4(3), 1498-1516.
- Lim, M., & Hastie, T. (2015). Learning interactions via hierarchical group-Lasso regularization. *Journal of Computational and Graphical Statistics*, 24(3), 627-654.
- Liu, J., Huang, J., Ma, S., & Wang, K. (2012). Incorporating group correlations in genome-wide association studies using smoothed group Lasso. *Biostatistics*, 14(2), 205-219.

- Liu, J., Huang, J., Zhang, Y., Lan, Q., Rothman, N., Zheng, T., and Ma, S. (2013). Identification of gene-environment interactions in cancer studies using penalization. *Genomics*, 102, 189-194.
- Michailidis, G. (2012). Statistical challenges in biological networks. *Journal of Computational and Graphical Statistics*, 21(4), 840-855.
- Reich, D. E., Cargill, M., Bolk, S., Ireland, J., Sabeti, P. C., Richter, D. J., ... & Lander, E. S. (2001). Linkage disequilibrium in the human genome. *Nature*, 411(6834), 199-204.
- She, Y., Wang, Z., & Jiang, H. (2018). Group regularized estimation under structural hierarchy. *Journal of the American Statistical Association*. 113, 445-454,
- Shi, X., Zhao, Q., Huang, J., Xie, Y., & Ma, S. (2015). Deciphering the associations between gene expression and copy number alteration using a sparse double Laplacian shrinkage approach. *Bioinformatics*, 31(24), 3977-3983.
- Shim, J., Hwang, C., Jeong, S., & Sohn, I. (2018). Semivarying coefficient least-squares support vector regression for analyzing high-dimensional gene-environmental data. *Journal of Applied Statistics*, 45(8), 1370-1381.
- Tibshirani, R., Saunders, M., Rosset, S., Zhu, J., & Knight, K. (2005). Sparsity and smoothness via the fused lasso. *Journal of the Royal Statistical Society: Series B (Statistical Methodology)*, 67(1), 91-108.
- Thomas, D. (2010). Gene-environment-wide association studies: emerging approaches. *Nature Reviews Genetics*, 11(4), 259-272.
- Wu, C., Cui, Y., & Ma, S. (2014). Integrative analysis of gene-environment interactions under a multi-response partially linear varying coefficient model. *Statistics in Medicine*, 33(28), 4988-4998.

- Wu, C., Shi, X., Cui, Y., & Ma, S. (2015). A penalized robust semiparametric approach for gene-environment interactions. *Statistics in Medicine*, 34(30), 4016-4030.
- Wu, C., Jiang, Y., Ren, J., Cui, Y., & Ma, S. (2018). Dissecting gene-environment interactions: A penalized robust approach accounting for hierarchical structures. *Statistics in Medicine*, 37(3), 437-456.
- Wu, M., & Ma, S. (2018). Robust genetic interaction analysis. *Briefings in Bioinformatics*. doi: 10.1093/bib/bby033
- Yu, G., & Liu, Y. (2016). Sparse regression incorporating graphical structure among predictors. *Journal of the American Statistical Association*, 111(514), 707-720.
- Zou, H., and Zhang, H. H. (2009). On the adaptive elastic-net with a diverging number of parameters. *Annals of Statistics*, 37(4), 1733-1751.

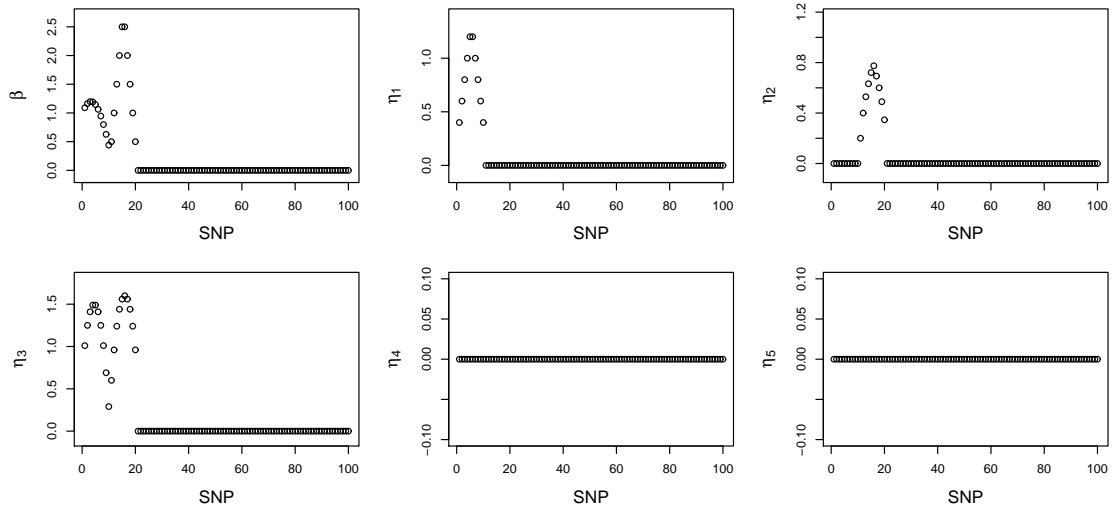


Figure 1: Simulation: true coefficient values for the main G effects and interactions. To improve presentation, only the first 100 effects are presented. The rest are zero.

Table 1: Simulation results under the linear model with MAF setting M1. In each cell, mean (sd) based on 500 replicates.

	M:TP	M:FP	I:TP	I:FP	RSSE	RSE	PMSE
AR(0.3)							
MA	0.1(0.5)	11.2(15.9)	2.2(2.2)	77.9(79.0)	15.03(5.07)	30.32(17.12)	28.36(8.80)
HierMCP	11.7(1.7)	68.5(11.4)	3.4(1.6)	4.2(2.0)	13.29(1.04)	26.48(2.53)	20.45(4.49)
SMCP	17.4(4.1)	2.7(5.2)	23.4(4.8)	19.7(14.3)	5.35(0.94)	2.65(0.67)	2.05(0.39)
Proposed	19.7(0.7)	0.0(0.1)	33.8(3.3)	4.1(2.5)	3.09(0.82)	2.32(0.66)	1.47(0.31)
AR(0.5)							
MA	0.4(1.0)	15.0(18.0)	4.8(3.7)	106.9(79.7)	20.15(8.82)	44.63(27.13)	40.81(16.31)
HierMCP	12.5(1.5)	78.1(13.7)	4.1(1.8)	5.3(2.5)	14.54(1.30)	30.51(3.10)	25.42(6.31)
SMCP	19.0(1.4)	3.0(5.2)	23.6(4.7)	20.4(16.5)	5.15(0.88)	2.71(0.67)	2.28(0.70)
Proposed	19.7(0.6)	0.0(0.3)	34.8(2.8)	3.1(2.0)	2.67(0.75)	2.39(0.69)	1.47(0.37)
Band1							
MA	0.2(0.8)	10.4(17.0)	1.9(2.3)	75.7(81.1)	13.42(3.38)	24.02(13.53)	24.63(6.17)
HierMCP	11.6(1.6)	70.3(10.5)	3.0(1.8)	4.0(2.0)	13.36(0.97)	26.30(2.41)	20.91(4.06)
SMCP	17.7(3.1)	3.5(5.8)	22.0(4.2)	20.8(15.3)	5.48(0.92)	2.71(0.60)	2.19(0.55)
Proposed	19.6(0.8)	0.0(0.4)	33.4(3.5)	4.3(2.9)	3.24(0.99)	2.40(0.72)	1.55(0.40)
Band2							
MA	0.2(0.5)	9.2(14.6)	3.1(3.1)	79.2(80.3)	15.09(4.99)	29.89(17.11)	34.68(10.47)
HierMCP	12.4(1.7)	76.1(14.2)	3.9(1.9)	5.4(2.9)	14.22(1.39)	29.54(3.48)	24.11(6.01)
SMCP	18.8(1.7)	2.2(3.8)	24.4(4.8)	18.8(14.1)	4.93(1.00)	2.72(0.60)	2.17(0.53)
Proposed	19.6(0.6)	0.0(0.0)	34.2(3.6)	3.4(2.2)	2.74(0.92)	2.40(0.77)	1.49(0.41)
LD(0.3)							
MA	0.2(0.7)	8.5(13.8)	3.0(2.8)	70.6(75.7)	14.40(4.10)	27.57(13.99)	27.24(7.68)
HierMCP	11.9(1.7)	93.7(10.8)	1.6(1.2)	1.6(1.3)	15.52(1.15)	32.24(2.91)	25.96(5.44)
SMCP	17.3(4.1)	3.0(4.7)	22.9(4.7)	15.4(12.1)	5.42(0.97)	2.68(0.59)	2.23(0.65)
Proposed	19.3(1.0)	0.0(0.1)	33.2(3.8)	3.5(2.6)	3.10(0.98)	2.44(0.73)	1.60(0.44)
LD(0.5)							
MA	0.4(1.1)	9.5(16.3)	5.0(3.9)	77.8(73.9)	16.15(5.37)	34.21(16.84)	33.86(10.10)
HierMCP	12.3(1.6)	109.5(14.8)	1.6(1.1)	2.1(1.4)	17.76(1.62)	38.96(4.07)	35.11(9.11)
SMCP	18.6(2.3)	2.4(3.6)	25.3(4.9)	15.7(14.0)	4.93(1.16)	2.61(0.59)	2.20(0.62)
Proposed	19.2(1.1)	0.1(0.4)	33.7(3.8)	2.7(2.6)	2.95(1.10)	2.60(0.89)	1.60(0.50)

Table 2: Simulation results under the linear model with MAF setting M2. In each cell, mean (sd) based on 500 replicates.

	M:TP	M:FP	I:TP	I:FP	RSSE	RSE	PMSE
AR(0.3)							
MA	0.1(0.5)	7.1(14.4)	2.0(2.1)	53.9(70.5)	11.20(1.62)	17.58(8.90)	23.30(5.04)
HierMCP	11.9(1.7)	64.4(11.0)	4.2(2.1)	5.7(2.3)	13.09(1.00)	26.28(2.37)	19.38(4.95)
SMCP	16.5(3.3)	6.5(9.9)	12.3(8.3)	68.7(25.9)	7.06(1.51)	3.56(1.05)	5.53(3.43)
Proposed	19.7(0.6)	0.0(0.1)	34.2(3.3)	4.0(2.2)	3.04(0.86)	2.26(0.53)	1.45(0.29)
AR(0.5)							
MA	0.3(0.9)	10.3(15.7)	4.0(3.6)	80.0(79.4)	14.89(4.30)	30.05(15.14)	36.06(12.01)
HierMCP	12.5(1.4)	70.2(14.1)	5.0(2.4)	7.3(3.5)	14.02(1.58)	29.43(3.89)	23.00(6.29)
SMCP	17.7(3.1)	4.9(8.1)	17.8(5.9)	54.8(26.8)	6.10(1.12)	3.06(0.83)	4.09(3.23)
Proposed	19.7(0.6)	0.4(2.8)	34.7(2.9)	3.5(2.5)	2.72(0.77)	2.45(0.78)	1.50(0.40)
Band1							
MA	0.1(0.8)	6.7(13.3)	1.6(2.1)	53.6(69.2)	10.56(1.14)	14.71(8.46)	22.79(4.91)
HierMCP	11.7(1.5)	64.7(10.1)	3.9(2.2)	5.2(2.7)	13.12(0.96)	25.96(2.44)	19.76(4.25)
SMCP	16.1(3.4)	7.0(10.8)	11.3(7.7)	74.1(23.7)	7.19(1.35)	3.59(0.92)	5.95(3.14)
Proposed	19.7(0.8)	1.0(4.3)	33.3(3.5)	5.1(4.7)	3.24(1.02)	2.51(0.83)	1.58(0.45)
Band2							
MA	0.1(0.5)	6.2(13.2)	2.6(2.8)	55.1(70.7)	11.86(2.08)	19.93(10.16)	29.94(7.08)
HierMCP	12.6(1.6)	69.6(17.0)	4.9(2.4)	6.8(2.9)	13.84(1.62)	28.73(3.97)	23.04(6.61)
SMCP	16.9(3.8)	5.2(8.8)	17.8(7.2)	59.3(24.8)	6.18(1.22)	3.09(0.83)	4.18(2.65)
Proposed	19.6(0.7)	1.2(5.7)	33.8(3.6)	4.1(4.0)	2.82(1.02)	2.55(0.92)	1.59(0.57)
LD(0.3)							
MA	0.2(0.7)	8.5(13.8)	3.0(2.8)	70.6(75.7)	14.40(4.10)	27.57(13.99)	27.24(7.68)
HierMCP	11.9(1.7)	93.7(10.8)	1.6(1.2)	1.6(1.3)	15.52(1.15)	32.24(2.91)	25.96(5.44)
SMCP	17.3(4.1)	3.0(4.7)	22.9(4.7)	15.2(12.2)	5.42(0.97)	2.67(0.59)	2.22(0.65)
Proposed	19.3(1.0)	0.0(0.1)	33.2(3.8)	3.5(2.6)	3.10(0.98)	2.44(0.73)	1.60(0.44)
LD(0.5)							
MA	0.4(1.1)	9.5(16.3)	5.0(3.9)	77.8(73.9)	16.15(5.37)	34.21(16.84)	33.86(10.10)
HierMCP	12.3(1.6)	109.5(14.8)	1.6(1.1)	2.1(1.4)	17.76(1.62)	38.96(4.07)	35.11(9.11)
SMCP	18.5(2.3)	2.3(3.5)	25.2(4.9)	15.5(14.0)	4.93(1.17)	2.60(0.59)	2.19(0.62)
Proposed	19.2(1.1)	0.1(0.4)	33.7(3.8)	2.7(2.6)	2.95(1.10)	2.60(0.89)	1.60(0.50)

Table 3: Analysis of the GENEVA diabetes data (NHS/HPFS) using the proposed approach: identified main effects and interactions.

SNP	Location	Gene*		age	famdb	act	trans	ceraf	heme
				-0.3331	0.1711	-0.2659	0.2185	-0.3332	0.5615
rs17090278	61679934	RP11-593F5.2	-0.0016						
rs10019557	61684734	RP11-593F5.2	-0.0019						
rs17090285	61695580	RP11-593F5.2	-0.0019						
rs17090286	61695978	RP11-593F5.2	-0.0016						
rs11731112	65554491	RP11-63H19.1	0.0015						
rs4355422	65557183	RP11-63H19.1	0.0015						
rs1430504	65681190	RP11-707A18.1	-0.0035						
rs6551878	65690589	RP11-707A18.1	-0.0056						
rs6823601	65691562	RP11-707A18.1	-0.0043						
rs13151560	67160442	MIR1269A	0.0025						
rs1858306	67161812	MIR1269A	0.0083	0.0021	0.002	-0.0013	0.0027		
rs10016795	67167064	MIR1269A	0.0174	0.0047	0.0074	-0.0054	0.0096	-0.0026	-0.0034
rs17087008	67188696	MIR1269A	0.0282	0.0049	0.0169	-0.0145	0.0213	-0.0046	-0.0119
rs12331987	67188980	MIR1269A	0.0373		0.0261	-0.0265	0.0308	-0.0056	-0.0256
rs10000219	67200024	MIR1269A	0.0405	-0.0105	0.0274	-0.0336	0.0304	-0.0028	-0.0357
rs4860208	67201368	MIR1269A	0.035	-0.0142	0.02	-0.0277	0.0197		-0.0301
rs1511286	67213473	MIR1269A	0.0215	-0.0077	0.0082	-0.0126	0.0072		-0.0139
rs1033095	67232011	RPS23P3	0.0064	-0.0012	0.0011	-0.0019			-0.002
rs11936928	67489994	RPS23P3	0.0014						
rs6838523	67494918	RPS23P3	0.0014						
rs10033058	69177408	YTHDC1	0.0055						
rs2293595	69178920	YTHDC1	0.0097						0.0031
rs12649108	69181942	YTHDC1	0.0095						0.0036
rs17089267	69183791	YTHDC1	0.0067						0.002
rs1730872	69189048	YTHDC1	0.0018						
rs1399247	70973970	CSN1S2AP	-0.0012						
rs1717600	70974315	CSN1S2AP	-0.0013						
rs11936367	72884978	NPFFR2	-0.0013						
rs7699403	72893324	NPFFR2	-0.0042						
rs6856651	72896457	NPFFR2	-0.0068	0.0013					-0.001
rs7654531	72900621	NPFFR2	-0.0079	0.0018					-0.0013
rs6824342	72903182	NPFFR2	-0.0074	0.0016					
rs6824703	72903318	NPFFR2	-0.0051						
rs7687603	72915996	NPFFR2	-0.002						
rs12649753	74940765	CXCL2	0.0092			-0.0023			0.0026
rs546829	74956372	CXCL2	0.0199	-0.0012	-0.0028	-0.012	0.0024	0.0027	0.0129
rs1837559	74959093	CXCL2	0.0257	-0.003	-0.0061	-0.0217	0.0033	0.0034	0.0226

Continued on the next page

Table 3: Continued from the previous page

SNP	Position	Gene		age	famdb	act	trans	ceraf	heme
rs9131	74963049	CXCL2	0.0232	-0.0038	-0.0066	-0.0196	0.0021	0.0011	0.0199
rs1866755	74978340	MTHFD2L	0.0156	-0.0024	-0.0038	-0.0098			0.0096
rs7686861	74998484	MTHFD2L	0.0064			-0.0019			0.0018
rs11737437	80262521	NAA11	-0.0019						
rs10004440	80272792	NAA11	-0.0043						
rs2903619	80281513	NAA11	-0.0056						
rs11731223	80290084	GK2	-0.0051						
rs6534350	80305179	GK2	-0.0025						
rs17003746	80314643	GK2	-0.0015						
rs11930550	80317724	GK2	-0.0019						
rs17003749	80317772	GK2	-0.0014						
rs7680648	82666782	RP11-689K5.3	-0.0018						
rs17561568	82667783	RP11-689K5.3	-0.0068	-0.0011					
rs35036928	82671170	RP11-689K5.3	-0.0137	-0.0036		-0.0026			-0.0032
rs4693369	82671234	RP11-689K5.3	-0.0156	-0.0046		-0.0027			-0.0049
rs12508164	82671299	RP11-689K5.3	-0.012	-0.0029		-0.001			-0.0038
rs7672440	82671938	RP11-689K5.3	-0.0079	-0.0013					-0.0018
rs1353661	82672523	RP11-689K5.3	-0.0025						
rs676592	82733530	RP11-689K5.3	-0.0012						
rs1993798	82762741	RP11-689K5.3	0.0047						
rs2868257	82762839	RP11-689K5.3	0.0072						
rs6535281	82763010	RP11-689K5.3	0.0048						
rs6535291	82926694	RP11-689K5.3	-0.0011						
rs434193	86253489	ARHGAP24	-0.0032						
rs6842681	86253994	ARHGAP24	-0.0084	0.0019		-0.0036	-0.0033		-0.0031
rs425196	86255297	ARHGAP24	-0.0144	0.0054		-0.0083	-0.0073		-0.0076
rs416035	86255366	ARHGAP24	-0.0203	0.0111	-0.0014	-0.014	-0.0117		-0.0136
rs432755	86255399	ARHGAP24	-0.0252	0.0174	-0.003	-0.0196	-0.016		-0.0196
rs375432	86255845	ARHGAP24	-0.0276	0.0214	-0.0041	-0.0224	-0.0185		-0.023
rs425642	86255997	ARHGAP24	-0.0257	0.0207	-0.0037	-0.0194	-0.016		-0.021
rs407430	86256356	ARHGAP24	-0.0204	0.0151	-0.0023	-0.0128	-0.0109		-0.0148
rs400023	86256538	ARHGAP24	-0.0131	0.0077		-0.0062	-0.0056		-0.0077
rs585787	86257453	ARHGAP24	-0.006	0.0023		-0.0019	-0.0019		-0.0025
rs380632	86264123	ARHGAP24	-0.0012						
rs2726516	106346206	PPA2	0.0022						
rs2636739	106352105	PPA2	0.0022						

* Genes that SNPs belong to or are the closest to.

Table 4: Analysis of the TCGA SKCM data using the proposed approach: identified main effects and interactions

Gene		Age	PN	Gender	Breslow's depth	Clark level
		-0.1381	-0.3077	0.0536	-0.2158	-0.1590
ACTL6B	-0.0067					
BLOC1S5	0.0188	-0.0012				
C3ORF67	0.0420	-0.0014	0.0064		0.0169	0.0016
CLEC2L	-0.0069					
CLPB	-0.0048					
CREG1	0.0281			-0.0018		
CRYBA1	-0.0037					
ENDOD1	0.0160		-0.0013	-0.0014		-0.0020
ETV3	-0.0019					
FAM131B	0.0041					
GOLPH3L	-0.0024					
IFNA7	-0.0018					
IL17A	0.0046					
IL17F	0.0143			-0.0014		
IL34	0.0030					
INPP5K	0.0093					
INTS4	-0.0055					
ISL2	-0.0022					
KCNE1	0.0281	-0.0026		0.0024		-0.0055
LAMTOR1	-0.0078					
LANCL2	0.0149					0.0012
LYNX1	-0.0261	0.0012	0.0021	-0.0011		-0.0026
MEPE	0.0144	-0.0012				-0.0014
METTL21C	0.0087					
NKAIN2	-0.0239	0.0019	0.0027		0.0013	0.0033
NKAIN3	-0.0019					
NOV	0.0422		-0.0070	-0.0085	-0.0060	0.0047
OR5L2	0.0452	-0.0103	-0.0064	-0.0103	-0.0037	0.0053
PRSS3	-0.0100					
PXDNL	-0.0106					
RAC1	-0.0177					0.0013
RAET1L	0.0093					
RIMS2	0.0076					
RPTN	-0.0023					
SERPINB13	-0.0079					
SERPINB3	-0.0018					

Continued on the next page

Table 4: Continued from the previous page

Gene	Age	PN	Gender	Breslow's depth	Clark level	
SETD3	0.0139					
SKIDA1	-0.0075					
SLFN13	0.0212	-0.0023				
SPINK4	0.0012					
SPRR2B	0.0015					
STMN4	0.0035					
STPG4	-0.0055					
SYT12	0.0027					
TAS2R1	-0.0056					
TRIM46	-0.0117					
UBE2V1	-0.0317	-0.0018	0.0045		0.0019	
UGT1A7	-0.0056					
WDPCP	-0.0843	-0.0194	-0.0322	-0.0018	0.0206	-0.0192
WDR77	-0.0137					

Appendix

Estimation under the AFT model

For subject i , denote T_i as the survival time of interest. Use notations similar to those in the main text. For T_i , consider the accelerated failure time (AFT) model

$$\log(T_i) = \alpha_0 + \sum_{k=1}^q Z_{ik}\alpha_k + \sum_{j=1}^p X_{ij}\beta_j + \sum_{k=1}^q \sum_{j=1}^p Z_{ik}X_{ij}\eta_{kj} + \varepsilon_i,$$

where α_0 is the intercept. In practice, right censoring is usually present. Denote C_i as the censoring time for subject i , then we observe $Y_i = \log(\min(T_i, C_i))$ and $\tilde{\delta}_i = I(T_i \leq C_i)$. Assume that data $\{(\mathbf{Z}_i, \mathbf{X}_i, Y_i, \tilde{\delta}_i), i = 1, \dots, n\}$ have been sorted according to Y_i from the smallest to the largest.

For estimation, the following weighted least squared loss function is adopted,

$$\frac{1}{2n} \sum_{i=1}^n w_i \left[Y_i - \left(\alpha_0 + \sum_{k=1}^q Z_{ik}\alpha_k + \sum_{j=1}^p X_{ij}\beta_j + \sum_{k=1}^q \sum_{j=1}^p Z_{ik}X_{ij}\eta_{kj} \right) \right]^2, \quad (\text{A1})$$

where w_i 's are the Kaplan-Meier weights defined as

$$w_1 = \frac{\tilde{\delta}_1}{n}, \quad w_i = \frac{\tilde{\delta}_i}{n-i+1} \prod_{l=1}^{i-1} \left(\frac{n-l}{n-l+1} \right)^{\tilde{\delta}_l}, \quad i = 2, \dots, n.$$

We center Y_i , \mathbf{Z}_i , \mathbf{X}_i , and $\mathbf{W}_i^{(k)} = (Z_{ik}X_{i1}, \dots, Z_{ik}X_{ip})$ using their weighted means. Specifically,

$$Y_i = \sqrt{w_i}(Y_i - \bar{Y}), \quad \mathbf{Z}_i = \sqrt{w_i}(\mathbf{Z}_i - \bar{\mathbf{Z}}), \quad \mathbf{X}_i = \sqrt{w_i}(\mathbf{X}_i - \bar{\mathbf{X}}), \quad \mathbf{W}_i^{(k)} = \sqrt{w_i}(\mathbf{W}_i^{(k)} - \bar{\mathbf{W}}^{(k)}),$$

where $\bar{Y} = \sum_{i=1}^n w_i Y_i / \sum_{i=1}^n w_i$, $\bar{\mathbf{Z}} = \sum_{i=1}^n w_i \mathbf{Z}_i / \sum_{i=1}^n w_i$, $\bar{\mathbf{X}} = \sum_{i=1}^n w_i \mathbf{X}_i / \sum_{i=1}^n w_i$, and $\bar{\mathbf{W}}^{(k)} = \sum_{i=1}^n w_i \mathbf{W}_i^{(k)} / \sum_{i=1}^n w_i$. Then, loss function (A1) can be rewritten as

$$\frac{1}{2n} \left\| \mathbf{Y} - \mathbf{Z}\boldsymbol{\alpha} - \mathbf{X}\boldsymbol{\beta} - \sum_{k=1}^q \mathbf{W}^{(k)}\boldsymbol{\eta}_k \right\|_2^2.$$

Details for Steps 2.1 and 2.2 of the proposed algorithm

Consider the objective function

$$\boldsymbol{\beta}^{(t)} = \operatorname{argmin} \frac{1}{2n} \left\| \tilde{\mathbf{Y}}^{(t)} - \tilde{\mathbf{X}}^{(t)} \boldsymbol{\beta} \right\|_2^2 + \sum_{j=1}^p \rho(|\beta_j|; \lambda_1, r) + \frac{1}{2} \lambda_2 (\boldsymbol{\beta}' \mathbf{J} \boldsymbol{\beta}).$$

For $j = 1, \dots, p$, the CD algorithm optimizes the objective function with respect to β_j while fixing the other parameters $\beta_l (l \neq j)$ at their current estimates $\beta_l^{(t)}$ for $l < j$ or $\beta_l^{(t-1)}$ for $l > j$. Specifically, consider the following simplified objective function

$$Q_s(\beta_j) = \frac{1}{2n} \left\| \mathbf{res}_{-j}^{(t)} - \tilde{\mathbf{X}}_j^{(t)} \beta_j \right\|_2^2 + \rho(|\beta_j|; \lambda_1, r) + \frac{1}{2} \lambda_2 \left(J_{jj} \beta_j^2 + 2 \sum_{l=1}^{j-1} \beta_l^{(t)} J_{jl} + 2 \sum_{l=j+1}^p \beta_l^{(t-1)} J_{jl} \right), \quad (\text{A2})$$

where $\mathbf{res}_{-j}^{(t)} = \tilde{\mathbf{Y}}^{(t)} - \sum_{l=1}^{j-1} \tilde{\mathbf{X}}_l^{(t)} \beta_l^{(t)} - \sum_{l=j+1}^p \tilde{\mathbf{X}}_l^{(t)} \beta_l^{(t-1)}$. The first order derivative of (A2) is

$$\begin{aligned} \frac{\partial Q_s(\beta_j)}{\partial \beta_j} &= -\frac{1}{n} \left(\tilde{\mathbf{X}}_j^{(t)} \right)' \mathbf{res}_{-j}^{(t)} + \frac{1}{n} \left(\tilde{\mathbf{X}}_j^{(t)} \right)' \tilde{\mathbf{X}}_j^{(t)} \beta_j + \lambda_1 \operatorname{sgn}(\beta_j) \begin{cases} 1 - \frac{|\beta_j|}{\lambda_1 r} & |\beta_j| \leq \lambda_1 r \\ 0 & |\beta_j| > \lambda_1 r \end{cases} + \lambda_2 J_{jj} \beta_j + \lambda_2 \Delta_j^{(t)}, \\ &\triangleq -\varphi_j^{(t)} + \chi_j^{(t)} \beta_j + \lambda_1 \operatorname{sgn}(\beta_j) \begin{cases} 1 - \frac{|\beta_j|}{\lambda_1 r} & |\beta_j| \leq \lambda_1 r \\ 0 & |\beta_j| > \lambda_1 r \end{cases} + \lambda_2 J_{jj} \beta_j + \lambda_2 \Delta_j^{(t)}, \end{aligned}$$

where

$$\varphi_j^{(t)} = \frac{1}{n} \left(\tilde{\mathbf{X}}_j^{(t)} \right)' \mathbf{res}_{-j}^{(t)}, \quad \chi_j^{(t)} = \frac{1}{n} \left(\tilde{\mathbf{X}}_j^{(t)} \right)' \tilde{\mathbf{X}}_j^{(t)}, \quad \Delta_j^{(t)} = \sum_{l=1}^{j-1} \beta_l^{(t)} J_{jl} + \sum_{l=j+1}^p \beta_l^{(t-1)} J_{jl}.$$

By setting the first order derivative equal to zero, we have

$$\beta_j^{(t)} = \begin{cases} \frac{\operatorname{ST}(\varphi_j^{(t)} - \lambda_2 \Delta_j^{(t)}, \lambda_1)}{\chi_j^{(t)} + \lambda_2 J_{jj} - \frac{1}{r}} & \left| \varphi_j^{(t)} - \lambda_2 \Delta_j^{(t)} \right| \leq \lambda_1 r (\chi_j^{(t)} + \lambda_2 J_{jj}) \\ \frac{\varphi_j^{(t)} - \lambda_2 \Delta_j^{(t)}}{\chi_j^{(t)} + \lambda_2 J_{jj}} & \left| \varphi_j^{(t)} - \lambda_2 \Delta_j^{(t)} \right| > \lambda_1 r (\chi_j^{(t)} + \lambda_2 J_{jj}) \end{cases},$$

where $\operatorname{ST}(\nu, \lambda_1) = \operatorname{sgn}(\nu) (|\nu| - \lambda_1)_+$ is the soft-thresholding operator.

Proof of Theorem 1

To prove Theorem 1, it suffices to show that under conditions (C1)-(C5), for a given ξ ,

$$P \left\{ \inf_{\boldsymbol{\theta}_{\mathcal{A}} \in \mathcal{N}_1} \tilde{Q}_n(\boldsymbol{\theta}_{\mathcal{A}}) > \tilde{Q}_n(\boldsymbol{\theta}_{\mathcal{A}}^0) \right\} \geq 1 - \xi,$$

where $\mathcal{N}_1 = \{\boldsymbol{\theta}_{\mathcal{A}} : \|\boldsymbol{\theta}_{\mathcal{A}} - \boldsymbol{\theta}_{\mathcal{A}}^0\|_2 = \delta_n\}$.

Let $\mathbf{w} = \left(\mathbf{g}'_{q \times 1}, \mathbf{u}'_{|\mathcal{A}_1| \times 1}, \mathbf{v}'_{1_{|\mathcal{A}_2^1|} \times 1}, \dots, \mathbf{v}'_{q_{|\mathcal{A}_2^q|} \times 1} \right)'$ with $\|\mathbf{w}\|_2 = 1$ and $\boldsymbol{\theta}_{\mathcal{A}} = \boldsymbol{\theta}_{\mathcal{A}}^0 + \delta_n \mathbf{w}$. Let $L_n(\boldsymbol{\theta}_{\mathcal{A}}) = \left\| \mathbf{Y} - \mathbf{Z}\boldsymbol{\alpha} - \mathbf{X}_{\mathcal{A}_1} \boldsymbol{\beta}_{\mathcal{A}_1} - \sum_{k=1}^q \mathbf{W}_{\mathcal{A}_2^k}^{(k)} (\boldsymbol{\beta}_{\mathcal{A}_2^k} \odot \boldsymbol{\gamma}_{k, \mathcal{A}_2^k}) \right\|_2^2$, then

$$\begin{aligned} D_n(\mathbf{w}) &= \tilde{Q}_n(\boldsymbol{\theta}_{\mathcal{A}}^0 + \delta_n \mathbf{w}) - \tilde{Q}_n(\boldsymbol{\theta}_{\mathcal{A}}^0) \\ &= \frac{1}{2n} L_n(\boldsymbol{\theta}_{\mathcal{A}}^0 + \delta_n \mathbf{w}) - \frac{1}{2n} L_n(\boldsymbol{\theta}_{\mathcal{A}}^0) \\ &\quad + \frac{1}{2} \lambda_2 (\boldsymbol{\beta}_{\mathcal{A}_1}^0 + \delta_n \mathbf{u})' \mathbf{J}_{\mathcal{A}_1, \mathcal{A}_1} (\boldsymbol{\beta}_{\mathcal{A}_1}^0 + \delta_n \mathbf{u}) - \frac{1}{2} \lambda_2 (\boldsymbol{\beta}_{\mathcal{A}_1}^0)' \mathbf{J}_{\mathcal{A}_1, \mathcal{A}_1} \boldsymbol{\beta}_{\mathcal{A}_1}^0 \\ &\quad + \frac{1}{2} \lambda_2 \sum_{k=1}^q (\boldsymbol{\gamma}_{\mathcal{A}_2^k}^0 + \delta_n \mathbf{v}_k)' \mathbf{J}_{\mathcal{A}_2^k, \mathcal{A}_2^k} (\boldsymbol{\gamma}_{\mathcal{A}_2^k}^0 + \delta_n \mathbf{v}_k) - \frac{1}{2} \lambda_2 \sum_{k=1}^q (\boldsymbol{\gamma}_{\mathcal{A}_2^k}^0)' \mathbf{J}_{\mathcal{A}_2^k, \mathcal{A}_2^k} \boldsymbol{\gamma}_{\mathcal{A}_2^k}^0. \end{aligned}$$

We have

$$\begin{aligned} I &\triangleq \frac{1}{2n} L_n(\boldsymbol{\theta}_{\mathcal{A}}^0 + \delta_n \mathbf{w}) - \frac{1}{2n} L_n(\boldsymbol{\theta}_{\mathcal{A}}^0) \\ &= \frac{1}{2n} \delta_n \mathbf{w}' (\nabla L_n(\boldsymbol{\theta}_{\mathcal{A}}) |_{\boldsymbol{\theta}_{\mathcal{A}}^0}) + \frac{1}{4n} \delta_n^2 \mathbf{w}' (\nabla^2 L_n(\boldsymbol{\theta}_{\mathcal{A}}) |_{\tilde{\boldsymbol{\theta}}_{\mathcal{A}}}) \mathbf{w} \\ &= \delta_n \mathbf{w}' \left[-\frac{1}{n} \mathbf{G}(\boldsymbol{\beta}_{\mathcal{A}_2}^0, \boldsymbol{\gamma}_{\mathcal{A}_1}^0)' \boldsymbol{\varepsilon} \right] \\ &\quad + \frac{1}{2} \delta_n^2 \mathbf{w}' \left[\frac{1}{n} \mathbf{G}(\tilde{\boldsymbol{\beta}}_{\mathcal{A}_2}, \tilde{\boldsymbol{\gamma}}_{\mathcal{A}_1})' \mathbf{G}(\tilde{\boldsymbol{\beta}}_{\mathcal{A}_2}, \tilde{\boldsymbol{\gamma}}_{\mathcal{A}_1}) + \frac{1}{n} \mathbf{F}(\tilde{\boldsymbol{\theta}}_{\mathcal{A}}) \right] \mathbf{w} \\ &\triangleq I_1 + I_2, \end{aligned}$$

where $\boldsymbol{\varepsilon} = \mathbf{Y} - \mathbf{Z}\boldsymbol{\alpha}^0 - \mathbf{X}_{\mathcal{A}_1} \boldsymbol{\beta}_{\mathcal{A}_1}^0 - \sum_{k=1}^q \mathbf{W}_{\mathcal{A}_2^k}^{(k)} (\boldsymbol{\beta}_{\mathcal{A}_2^k}^0 \odot \boldsymbol{\gamma}_{k, \mathcal{A}_2^k}^0)$, $\boldsymbol{\gamma}_{\mathcal{A}_1} = (\boldsymbol{\gamma}'_{1, \mathcal{A}_1}, \dots, \boldsymbol{\gamma}'_{q, \mathcal{A}_1})'$ with $\gamma_{kj} = 0$, if $j \in \mathcal{A}_1$ but $j \notin \mathcal{A}_2^k$,

$$\mathbf{G}(\boldsymbol{\beta}_{\mathcal{A}_2}, \boldsymbol{\gamma}_{\mathcal{A}_1}) = \left(\mathbf{Z}, \mathbf{U}(\boldsymbol{\gamma}_{\mathcal{A}_1}), \mathbf{V}^{(1)}(\boldsymbol{\beta}_{\mathcal{A}_2^1}), \mathbf{V}^{(2)}(\boldsymbol{\beta}_{\mathcal{A}_2^2}), \dots, \mathbf{V}^{(q)}(\boldsymbol{\beta}_{\mathcal{A}_2^q}) \right)_{n \times (q+s)},$$

with

$$\mathbf{U}(\boldsymbol{\gamma}_{\mathcal{A}_1}) = \mathbf{X}_{\mathcal{A}_1} + \sum_{k=1}^q \mathbf{W}_{\mathcal{A}_1}^{(k)} \odot (\mathbf{1}_{n \times 1} (\boldsymbol{\gamma}_{k, \mathcal{A}_1})'), \quad \mathbf{V}^{(k)}(\boldsymbol{\beta}_{\mathcal{A}_2^k}) = \mathbf{W}_{\mathcal{A}_2^k}^{(k)} \odot \left(\mathbf{1}_{n \times 1} (\boldsymbol{\beta}_{\mathcal{A}_2^k})' \right),$$

$F(\boldsymbol{\theta}_{\mathcal{A}}) = (f_{jl}(\boldsymbol{\theta}_{\mathcal{A}}))_{(q+s) \times (q+s)}$ with $f_{jl}(\boldsymbol{\theta}_{\mathcal{A}}) = -\left(\mathbf{W}_{\zeta}^{(k)}\right)' (\mathbf{Y} - \mathbf{Z}\boldsymbol{\alpha} - \mathbf{X}_{\mathcal{A}_1}\boldsymbol{\beta}_{\mathcal{A}_1} - \sum_{g=1}^q \mathbf{W}_{\mathcal{A}_2^g}^{(g)}(\boldsymbol{\beta}_{\mathcal{A}_2^g} \odot \boldsymbol{\gamma}_{g, \mathcal{A}_2^g}))$ if both j and l correspond to the ζ th element of \mathcal{A}_2^k , and 0 otherwise, and $\tilde{\boldsymbol{\theta}}_{\mathcal{A}}$ lies on the line segment joining $\boldsymbol{\theta}_{\mathcal{A}}$ and $\boldsymbol{\theta}_{\mathcal{A}}^0$. Moreover,

$$\begin{aligned}
II &\triangleq \frac{1}{2}\lambda_2(\boldsymbol{\beta}_{\mathcal{A}_1}^0 + \delta_n \mathbf{u})' \mathbf{J}_{\mathcal{A}_1, \mathcal{A}_1}(\boldsymbol{\beta}_{\mathcal{A}_1}^0 + \delta_n \mathbf{u}) - \frac{1}{2}\lambda_2(\boldsymbol{\beta}_{\mathcal{A}_1}^0)' \mathbf{J}_{\mathcal{A}_1, \mathcal{A}_1} \boldsymbol{\beta}_{\mathcal{A}_1}^0 \\
&+ \frac{1}{2}\lambda_2 \sum_{k=1}^q (\boldsymbol{\gamma}_{\mathcal{A}_2^k}^0 + \delta_n \mathbf{v}_k)' \mathbf{J}_{\mathcal{A}_2^k, \mathcal{A}_2^k}(\boldsymbol{\gamma}_{\mathcal{A}_2^k}^0 + \delta_n \mathbf{v}_k) - \frac{1}{2}\lambda_2 \sum_{k=1}^q (\boldsymbol{\gamma}_{\mathcal{A}_2^k}^0)' \mathbf{J}_{\mathcal{A}_2^k, \mathcal{A}_2^k} \boldsymbol{\gamma}_{\mathcal{A}_2^k}^0 \\
&= \delta_n \lambda_2 \mathbf{w}' \tilde{\mathbf{J}}_{\mathcal{A}, \mathcal{A}} \boldsymbol{\theta}_{\mathcal{A}}^0 + \frac{1}{2} \delta_n^2 \lambda_2 \mathbf{w}' \tilde{\mathbf{J}}_{\mathcal{A}, \mathcal{A}} \mathbf{w} \\
&\geq -\delta_n \lambda_2 \|\tilde{\mathbf{J}}_{\mathcal{A}, \mathcal{A}} \boldsymbol{\theta}_{\mathcal{A}}^0\|_2,
\end{aligned}$$

where $\tilde{\mathbf{J}}_{\mathcal{A}, \mathcal{A}} = \text{diag}\left(\mathbf{0}_{q \times q}, \mathbf{J}_{\mathcal{A}_1, \mathcal{A}_1}, \dots, \mathbf{J}_{\mathcal{A}_2^q, \mathcal{A}_2^q}\right)$ is a block diagonal matrix with the diagonal blocks being $\mathbf{0}_{q \times q}, \mathbf{J}_{\mathcal{A}_1, \mathcal{A}_1}, \dots$, and $\mathbf{J}_{\mathcal{A}_2^g, \mathcal{A}_2^g}$, and $\frac{1}{2} \delta_n^2 \lambda_2 \mathbf{w}' \tilde{\mathbf{J}}_{\mathcal{A}, \mathcal{A}} \mathbf{w} \geq \frac{1}{2} \delta_n^2 \lambda_2 \lambda_{\min}(\tilde{\mathbf{J}}_{\mathcal{A}, \mathcal{A}}) \geq 0$ with condition (C5).

With $\delta_n = \frac{4\lambda_2 \|\tilde{\mathbf{J}}_{\mathcal{A}, \mathcal{A}} \boldsymbol{\theta}_{\mathcal{A}}^0\|_2}{\underline{c}} + E\sqrt{s/n}$, and conditions (C2), (C4) and (C5), we have

$$\|\tilde{\boldsymbol{\theta}}_{\mathcal{A}} - \boldsymbol{\theta}_{\mathcal{A}}^0\|_{\infty} \leq \|\boldsymbol{\theta}_{\mathcal{A}} - \boldsymbol{\theta}_{\mathcal{A}}^0\|_{\infty} \leq \delta_n < b_0/2.$$

Then, with condition (C3), we have

$$I_2 \geq \frac{1}{2} \delta_n^2 \underline{c} > 0.$$

For I_1 , with conditions (C1) and (C3), we have

$$\begin{aligned}
&P\left(\delta_n \mathbf{w}' \left[-\frac{1}{n} \mathbf{G}(\boldsymbol{\beta}_{\mathcal{A}_2}^0, \boldsymbol{\gamma}_{\mathcal{A}_1}^0)' \boldsymbol{\varepsilon}\right] \leq -\delta_n \epsilon\right) \\
&= P\left(\frac{\mathbf{w}' \left[-\frac{1}{n} \mathbf{G}(\boldsymbol{\beta}_{\mathcal{A}_2}^0, \boldsymbol{\gamma}_{\mathcal{A}_1}^0)' \boldsymbol{\varepsilon}\right]}{\left\|\mathbf{w}' \left[-\frac{1}{n} \mathbf{G}(\boldsymbol{\beta}_{\mathcal{A}_2}^0, \boldsymbol{\gamma}_{\mathcal{A}_1}^0)'\right]\right\|_2} \leq -\frac{\epsilon}{\left\|\mathbf{w}' \left[-\frac{1}{n} \mathbf{G}(\boldsymbol{\beta}_{\mathcal{A}_2}^0, \boldsymbol{\gamma}_{\mathcal{A}_1}^0)'\right]\right\|_2}\right) \\
&\leq \exp\left(-\frac{n\epsilon^2}{2\sigma^2 \bar{c}_s}\right).
\end{aligned}$$

Set $\epsilon = \frac{1}{4} \underline{c} \delta_n$, we have

$$P\left(\delta_n \mathbf{w}' \left[-\frac{1}{n} \mathbf{G}(\boldsymbol{\beta}_{\mathcal{A}_2}^0, \boldsymbol{\gamma}_{\mathcal{A}_1}^0)' \boldsymbol{\varepsilon}\right] \geq -\frac{1}{4} \underline{c} \delta_n^2\right) \geq 1 - \exp\left(-\frac{n\underline{c}^2 \delta_n^2}{32\sigma^2 \bar{c}_s}\right).$$

Thus, with $\delta_n = \frac{4\lambda_2\|\tilde{\mathbf{J}}_{\mathcal{A},\mathcal{A}}\boldsymbol{\theta}_{\mathcal{A}}^0\|_2}{\underline{c}} + E\sqrt{s/n}$, we have

$$\begin{aligned}
P\left\{\inf_{\hat{\boldsymbol{\theta}}\in\mathcal{N}_1} Q_n(\hat{\boldsymbol{\theta}}) > Q_n(\boldsymbol{\theta}^0)\right\} &\geq P\{D_n(\mathbf{w}) > 0\} \\
&\geq P\left\{\delta_n\mathbf{w}'\left[-\frac{1}{n}\mathbf{G}(\boldsymbol{\beta}_{\mathcal{A}_2}^0, \boldsymbol{\gamma}_{\mathcal{A}_1}^0)'\boldsymbol{\varepsilon}\right] + \frac{1}{2}\delta_n^2\underline{c} - \delta_n\lambda_2\|\tilde{\mathbf{J}}_{\mathcal{A},\mathcal{A}}\boldsymbol{\theta}_{\mathcal{A}}^0\|_2 > 0\right\} \\
&\geq P\left(\delta_n\mathbf{w}'\left[-\frac{1}{n}\mathbf{G}(\boldsymbol{\beta}_{\mathcal{A}_2}^0, \boldsymbol{\gamma}_{\mathcal{A}_1}^0)'\boldsymbol{\varepsilon}\right] \geq -\frac{1}{4}\underline{c}\delta_n^2\right) \\
&\geq 1 - \exp\left(-\frac{n\underline{c}^2\delta_n^2}{32\sigma^2\bar{c}s}\right) \\
&= 1 - \exp\left(-\frac{\left[4\sqrt{n/s}\lambda_2\|\tilde{\mathbf{J}}_{\mathcal{A},\mathcal{A}}\boldsymbol{\theta}_{\mathcal{A}}^0\|_2 + E\underline{c}\right]^2}{32\sigma^2\bar{c}}\right).
\end{aligned}$$

This completes the proof of Theorem 1.

Proof of Theorem 2

First, consider $\hat{\beta}_{\mathcal{A}_1^c}$. Following Theorem 1 in Fan and Lv (2011), with condition (C9) and Theorem 1, it suffices to check condition (8) in Fan and Lv (2011). Let

$$h_1 = (n\lambda_1)^{-1} \left[\frac{1}{2} \nabla_{\beta_{\mathcal{A}_1^c}} L_n(\boldsymbol{\theta}) \Big|_{\hat{\boldsymbol{\theta}}} + \lambda_2 n \mathbf{J}_{\mathcal{A}_1^c} \hat{\boldsymbol{\beta}} \right].$$

Since $\hat{\beta}_{\mathcal{A}_1^c} = 0$, with a Taylor expansion, we have

$$\begin{aligned} h_1 &= (n\lambda_1)^{-1} \left[-\mathbf{U}(\gamma_{\mathcal{A}_1^c})' \left(\mathbf{Y} - \mathbf{Z}\hat{\boldsymbol{\alpha}} - \mathbf{X}\hat{\boldsymbol{\beta}} - \sum_{k=1}^q \mathbf{W}^{(k)}(\hat{\boldsymbol{\beta}} \odot \hat{\boldsymbol{\gamma}}_k) \right) + \lambda_2 n \mathbf{J}_{\mathcal{A}_1^c, \mathcal{A}_1} \hat{\boldsymbol{\beta}}_{\mathcal{A}_1} \right] \\ &= (n\lambda_1)^{-1} \left[-\mathbf{U}(\gamma_{\mathcal{A}_1^c}^0)' \boldsymbol{\varepsilon} + \mathbf{U}(\gamma_{\mathcal{A}_1^c}^0)' \mathbf{G}(\beta_{\mathcal{A}_2}^0, \gamma_{\mathcal{A}_1}^0)' (\hat{\boldsymbol{\theta}}_{\mathcal{A}} - \boldsymbol{\theta}_{\mathcal{A}}^0) + \boldsymbol{\kappa} + \lambda_2 n \mathbf{J}_{\mathcal{A}_1^c, \mathcal{A}_1} \hat{\boldsymbol{\beta}}_{\mathcal{A}_1} \right] \\ &= (n\lambda_1)^{-1} \left[-\mathbf{U}(\gamma_{\mathcal{A}_1^c}^0)' \boldsymbol{\varepsilon} + III + \lambda_2 n \mathbf{J}_{\mathcal{A}_1^c, \mathcal{A}_1} \hat{\boldsymbol{\beta}}_{\mathcal{A}_1} \right]. \end{aligned}$$

For *III*, let $m_j(\boldsymbol{\theta}_{\mathcal{A}}) = \left(\mathbf{X}_j + \sum_{k=1}^q \mathbf{W}_j^{(k)} \gamma_{kj} \right)' \left(\mathbf{Z}\boldsymbol{\alpha} + \mathbf{X}_{\mathcal{A}_1} \boldsymbol{\beta}_{\mathcal{A}_1} + \sum_{k=1}^q \mathbf{W}_{\mathcal{A}_2^k}^{(k)} (\boldsymbol{\beta}_{\mathcal{A}_2^k} \odot \gamma_{k, \mathcal{A}_2^k}) \right)$. Then $\boldsymbol{\kappa} = (\kappa_j, j \in \mathcal{A}_1^c)'$ with

$$\begin{aligned} \kappa_j &= \frac{1}{2} (\hat{\boldsymbol{\theta}}_{\mathcal{A}} - \boldsymbol{\theta}_{\mathcal{A}}^0)' \left(\nabla_{\boldsymbol{\theta}_{\mathcal{A}}}^2 m_j(\boldsymbol{\theta}_{\mathcal{A}}) \Big|_{\hat{\boldsymbol{\theta}}_{\mathcal{A}}} \right) (\hat{\boldsymbol{\theta}}_{\mathcal{A}} - \boldsymbol{\theta}_{\mathcal{A}}^0), \\ &\leq \max_j \frac{1}{2} \lambda_{\max} \left(\mathbf{T}_1^{(j)}(\tilde{\boldsymbol{\gamma}}_j) \right) \|\boldsymbol{\theta}_{\mathcal{A}}^* - \boldsymbol{\theta}_{\mathcal{A}}^0\|_2, \end{aligned}$$

where $\tilde{\boldsymbol{\theta}}_{\mathcal{A}}$ lies on the line segment jointing $\boldsymbol{\theta}_{\mathcal{A}}^*$ and $\boldsymbol{\theta}_{\mathcal{A}}^0$. Here $\mathbf{T}_1^{(j)}(\boldsymbol{\gamma}_j) = \left(t_{lh}^{(j)}(\boldsymbol{\gamma}_j) \right)_{(q+s) \times (q+s)}$ with $t_{lh}^{(j)}(\boldsymbol{\gamma}_j) = \left(\mathbf{X}_j + \sum_{g=1}^q \mathbf{W}_j^{(g)} \gamma_{gj} \right)' \mathbf{W}_{\zeta}^{(k)}$, if both l and h correspond to the ζ th element of \mathcal{A}_2^k , and 0 otherwise. Consider the event

$$\Omega_1 = \left\{ \|\mathbf{U}(\gamma_{\mathcal{A}_1^c}^0)' \boldsymbol{\varepsilon}\|_{\infty} \leq \zeta_n \sqrt{n} \right\},$$

with $\zeta_n = n^a (\log(n))^{1/2}$. With conditions (C6) and (C7), we have

$$\begin{aligned} P(\Omega_1) &= 1 - P \left\{ \|\mathbf{U}(\gamma_{\mathcal{A}_1^c}^0)' \boldsymbol{\varepsilon}\|_{\infty} > \zeta_n \sqrt{n} \right\} \\ &\geq 1 - \sum_{j \in \mathcal{A}_1^c} P \left\{ \|\mathbf{U}(\gamma_j^0)' \boldsymbol{\varepsilon}\| > \zeta_n \sqrt{n} \right\} \\ &\geq 1 - 2(p - s_0) \exp \left(- \frac{\zeta_n^2 n}{2\sigma^2 \max_{j \in \mathcal{A}_1^c} \|\mathbf{U}(\gamma_j^0)\|_2^2} \right) \end{aligned}$$

$$\geq 1 - 2p \exp\left(-\frac{\zeta_n^2 n}{2\sigma^2 \max_{j \in \mathcal{A}_1^c} \|\mathbf{U}(\gamma_j^0)\|_2^2}\right) \rightarrow 1,$$

as $\log(p) = O(n^a)$ and $\|\mathbf{U}(\gamma_j^0)\|_2 = O(\sqrt{n})$. Thus, with probability tending to 1,

$$\|\mathbf{U}(\gamma_{\mathcal{A}_1^c}^0)' \boldsymbol{\varepsilon}\|_\infty = O(n^{a/2+1/2} \sqrt{\log n}).$$

Then, condition (C8) gives

$$(n\lambda_1)^{-1} \|\mathbf{U}(\gamma_{\mathcal{A}_1^c}^0)' \boldsymbol{\varepsilon}\|_\infty = o(1).$$

For *III*, with conditions (C6) and (C8),

$$\begin{aligned} (n\lambda_1)^{-1} \|\text{III}\|_\infty &= (n\lambda_1)^{-1} \left[\|\mathbf{U}(\gamma_{\mathcal{A}_1^c}^0)' \mathbf{G}(\boldsymbol{\beta}_{\mathcal{A}_2}^0, \boldsymbol{\gamma}_{\mathcal{A}_1}^0)' (\hat{\boldsymbol{\theta}}_{\mathcal{A}} - \boldsymbol{\theta}_{\mathcal{A}}^0)\|_\infty + \|\boldsymbol{\kappa}\|_\infty \right] \\ &= (n\lambda_1)^{-1} \left[O(n) \|\boldsymbol{\theta}_{\mathcal{A}}^* - \boldsymbol{\theta}_{\mathcal{A}}^0\|_2 + O(n) \|\boldsymbol{\theta}_{\mathcal{A}}^* - \boldsymbol{\theta}_{\mathcal{A}}^0\|_2^2 \right] \\ &= O(\lambda_1^{-1} \sqrt{s/n}) = o(1). \end{aligned}$$

With conditions (C4), (C5) and (C8),

$$\begin{aligned} (n\lambda_1)^{-1} \|\lambda_2 n \mathbf{J}_{\mathcal{A}_1^c, \mathcal{A}_1} \hat{\boldsymbol{\beta}}_{\mathcal{A}_1}\|_\infty &= (\lambda_1)^{-1} \|\lambda_2 \mathbf{J}_{\mathcal{A}_1^c, \mathcal{A}_1} \boldsymbol{\beta}_{\mathcal{A}_1}^0 - \lambda_2 \mathbf{J}_{\mathcal{A}_1^c, \mathcal{A}_1} (\hat{\boldsymbol{\beta}}_{\mathcal{A}_1} - \boldsymbol{\beta}_{\mathcal{A}_1}^0)\|_\infty \\ &\leq (\lambda_1)^{-1} \|\lambda_2 \mathbf{J}_{\mathcal{A}_1^c, \mathcal{A}_1} \boldsymbol{\beta}_{\mathcal{A}_1}^0\|_\infty + (\lambda_1)^{-1} \|\lambda_2 \mathbf{J}_{\mathcal{A}_1^c, \mathcal{A}_1} (\hat{\boldsymbol{\beta}}_{\mathcal{A}_1} - \boldsymbol{\beta}_{\mathcal{A}_1}^0)\|_\infty \\ &= O(\lambda_1^{-1} \sqrt{s/n}) = o(1). \end{aligned}$$

Next, consider $\hat{\boldsymbol{\gamma}}_{k, (\tilde{\mathcal{A}}_2^k)^c}$. A similar process is adopted to check condition (8) in Fan and Lv (2011). Let

$$h_2 = (n\lambda_1)^{-1} \left[\frac{1}{2} \nabla_{(\tilde{\mathcal{A}}_2^k)^c} L_n(\boldsymbol{\theta}) \Big|_{\hat{\boldsymbol{\theta}}} + \lambda_2 n \mathbf{J}_{(\tilde{\mathcal{A}}_2^k)^c} \hat{\boldsymbol{\gamma}}_k \right].$$

Since $\hat{\boldsymbol{\gamma}}_{(\tilde{\mathcal{A}}_2^k)^c} = 0$ and $\hat{\boldsymbol{\beta}}_{(\tilde{\mathcal{A}}_2^k)^c} \neq 0$, with a Taylor expansion, we have

$$\begin{aligned} h_2 &= (n\lambda_1)^{-1} \left[-\mathbf{V}^{(k)}(\boldsymbol{\beta}_{(\tilde{\mathcal{A}}_2^k)^c})' \left(\mathbf{Y} - \mathbf{Z}\hat{\boldsymbol{\alpha}} - \mathbf{X}\hat{\boldsymbol{\beta}} - \sum_{k=1}^q \mathbf{W}^{(k)}(\hat{\boldsymbol{\beta}} \odot \hat{\boldsymbol{\gamma}}_k) \right) + \lambda_2 n \mathbf{J}_{(\tilde{\mathcal{A}}_2^k)^c} \hat{\boldsymbol{\gamma}}_k \right] \\ &= (n\lambda_1)^{-1} \left[-\mathbf{V}^{(k)}(\boldsymbol{\beta}_{(\tilde{\mathcal{A}}_2^k)^c}^0)' \boldsymbol{\varepsilon} + \mathbf{V}^{(k)}(\boldsymbol{\beta}_{(\tilde{\mathcal{A}}_2^k)^c}^0)' \mathbf{G}(\boldsymbol{\beta}_{\mathcal{A}_2}^0, \boldsymbol{\gamma}_{\mathcal{A}_1}^0)' (\hat{\boldsymbol{\theta}}_{\mathcal{A}} - \boldsymbol{\theta}_{\mathcal{A}}^0) + \tilde{\boldsymbol{\kappa}} + \lambda_2 n \mathbf{J}_{(\tilde{\mathcal{A}}_2^k)^c} \hat{\boldsymbol{\gamma}}_k \right] \\ &= (n\lambda_1)^{-1} \left[-\mathbf{V}^{(k)}(\boldsymbol{\beta}_{(\tilde{\mathcal{A}}_2^k)^c}^0)' \boldsymbol{\varepsilon} + IV + \lambda_2 n \mathbf{J}_{(\tilde{\mathcal{A}}_2^k)^c, \mathcal{A}_2^k} \hat{\boldsymbol{\gamma}}_{k, \mathcal{A}_2^k} \right]. \end{aligned}$$

For *IV*, let $\tilde{m}_j(\boldsymbol{\theta}_{\mathcal{A}}) = \left(\mathbf{W}_j^{(k)}\beta_j\right)' \left(\mathbf{Z}\boldsymbol{\alpha} + \mathbf{X}_{\mathcal{A}_1}\boldsymbol{\beta}_{\mathcal{A}_1} + \sum_{k=1}^q \mathbf{W}_{\mathcal{A}_2^k}^{(k)}(\boldsymbol{\beta}_{\mathcal{A}_2^k} \odot \boldsymbol{\gamma}_{k,\mathcal{A}_2^k})\right)$, then $\tilde{\boldsymbol{\kappa}} = (\tilde{\kappa}_j, j \in (\tilde{\mathcal{A}}_2^k)^c)'$ with

$$\begin{aligned}\tilde{\kappa}_j &= \frac{1}{2}(\hat{\boldsymbol{\theta}}_{\mathcal{A}} - \boldsymbol{\theta}_{\mathcal{A}}^0) \left(\nabla_{\boldsymbol{\theta}_{\mathcal{A}}}^2 \tilde{m}_j(\boldsymbol{\theta}_{\mathcal{A}}) \Big|_{\hat{\boldsymbol{\theta}}_{\mathcal{A}}} \right) (\hat{\boldsymbol{\theta}}_{\mathcal{A}} - \boldsymbol{\theta}_{\mathcal{A}}^0), \\ &\leq \max_j \frac{1}{2} \lambda_{\max} \left(\mathbf{T}_2^{(j)}(\tilde{\beta}_j) \right) \|\boldsymbol{\theta}_{\mathcal{A}}^* - \boldsymbol{\theta}_{\mathcal{A}}^0\|_2,\end{aligned}$$

where $\tilde{\boldsymbol{\theta}}_{\mathcal{A}}$ lies on the line segment jointing $\boldsymbol{\theta}_{\mathcal{A}}^*$ and $\boldsymbol{\theta}_{\mathcal{A}}^0$. Here $\mathbf{T}_2^{(j)}(\beta_j) = \left(t_{lh}^{(j)}(\beta_j)\right)_{(q+s) \times (q+s)}$ with $t_{lh}^{(j)}(\beta_j) = \left(\mathbf{W}_j^{(k)}\beta_j\right)' \mathbf{W}_{\zeta}^{(k)}$ if both l and h correspond to the ζ th element of \mathcal{A}_2^k , and 0 otherwise.

Consider the event

$$\Omega_2 = \left\{ \|\mathbf{V}^{(k)}(\boldsymbol{\beta}_{(\tilde{\mathcal{A}}_2^k)^c}^0)'\boldsymbol{\varepsilon}\|_{\infty} \leq \zeta_n \sqrt{n} \right\},$$

with $\zeta_n = n^a(\log(n))^{1/2}$. We have

$$\begin{aligned}P(\Omega_2) &= 1 - P \left\{ \|\mathbf{V}^{(k)}(\boldsymbol{\beta}_{(\tilde{\mathcal{A}}_2^k)^c}^0)'\boldsymbol{\varepsilon}\|_{\infty} > \zeta_n \sqrt{n} \right\} \\ &\geq 1 - \sum_{j \in (\tilde{\mathcal{A}}_2^k)^c} P \left\{ \|\mathbf{V}^{(k)}(\beta_j^0)'\boldsymbol{\varepsilon}\| > \zeta_n \sqrt{n} \right\} \\ &\geq 1 - 2p \exp \left(-\frac{\zeta_n^2 n}{2\sigma^2 \max_{j \in (\tilde{\mathcal{A}}_2^k)^c} \|\mathbf{V}^{(k)}(\beta_j^0)\|_2^2} \right) \rightarrow 1,\end{aligned}$$

as $\log(p) = O(n^a)$ and $\|\mathbf{V}^{(k)}(\beta_j^0)\|_2 = O(\sqrt{n})$. Thus, we have, with probability tending to 1,

$$\|\mathbf{V}^{(k)}(\boldsymbol{\beta}_{(\tilde{\mathcal{A}}_2^k)^c}^0)'\boldsymbol{\varepsilon}\|_{\infty} = O(n^{a/2+1/2} \sqrt{\log n}).$$

The condition (C8) gives

$$(n\lambda_1)^{-1} \|\mathbf{V}^{(k)}(\boldsymbol{\beta}_{(\tilde{\mathcal{A}}_2^k)^c}^0)'\boldsymbol{\varepsilon}\|_{\infty} = o(1).$$

For *IV*, with conditions (C6) and (C8),

$$\begin{aligned}(n\lambda_1)^{-1} \|IV\|_{\infty} &= (n\lambda_1)^{-1} \left[\|\mathbf{V}^{(k)}(\boldsymbol{\beta}_{(\tilde{\mathcal{A}}_2^k)^c}^0)'\mathbf{G}(\boldsymbol{\beta}_{\mathcal{A}_2}^0, \boldsymbol{\gamma}_{\mathcal{A}_1}^0)'(\hat{\boldsymbol{\theta}}_{\mathcal{A}} - \boldsymbol{\theta}_{\mathcal{A}}^0)\|_{\infty} + \|\tilde{\boldsymbol{\kappa}}\|_{\infty} \right] \\ &= (n\lambda_1)^{-1} \left[O(n) \|\boldsymbol{\theta}_{\mathcal{A}}^* - \boldsymbol{\theta}_{\mathcal{A}}^0\|_2 + O(n) \|\boldsymbol{\theta}_{\mathcal{A}}^* - \boldsymbol{\theta}_{\mathcal{A}}^0\|_2^2 \right] \\ &= O(\lambda_1^{-1} \sqrt{s/n}) = o(1).\end{aligned}$$

With conditions (C4), (C5) and (C8),

$$\begin{aligned}
(\lambda_1)^{-1} \|\lambda_2 \mathbf{J}_{(\bar{\mathcal{A}}_2^k)^c, \mathcal{A}_2^k} \hat{\boldsymbol{\gamma}}_{k, \mathcal{A}_2^k}\|_\infty &= (\lambda_1)^{-1} \|\lambda_2 \mathbf{J}_{(\bar{\mathcal{A}}_2^k)^c, \mathcal{A}_2^k} \boldsymbol{\gamma}_{k, \mathcal{A}_2^k}^0 - \lambda_2 \mathbf{J}_{(\bar{\mathcal{A}}_2^k)^c, \mathcal{A}_2^k} (\hat{\boldsymbol{\gamma}}_{k, \mathcal{A}_2^k} - \boldsymbol{\gamma}_{k, \mathcal{A}_2^k}^0)\|_\infty \\
&\leq (\lambda_1)^{-1} \|\lambda_2 \mathbf{J}_{(\bar{\mathcal{A}}_2^k)^c, \mathcal{A}_2^k} \boldsymbol{\gamma}_{k, \mathcal{A}_2^k}^0\|_\infty + (\lambda_1)^{-1} \|\lambda_2 \mathbf{J}_{(\bar{\mathcal{A}}_2^k)^c, \mathcal{A}_2^k} (\hat{\boldsymbol{\gamma}}_{k, \mathcal{A}_2^k} - \boldsymbol{\gamma}_{k, \mathcal{A}_2^k}^0)\|_\infty \\
&= O(\lambda_1^{-1} \sqrt{s/n}) = o(1).
\end{aligned}$$

This completes the proof.

Additional numerical results

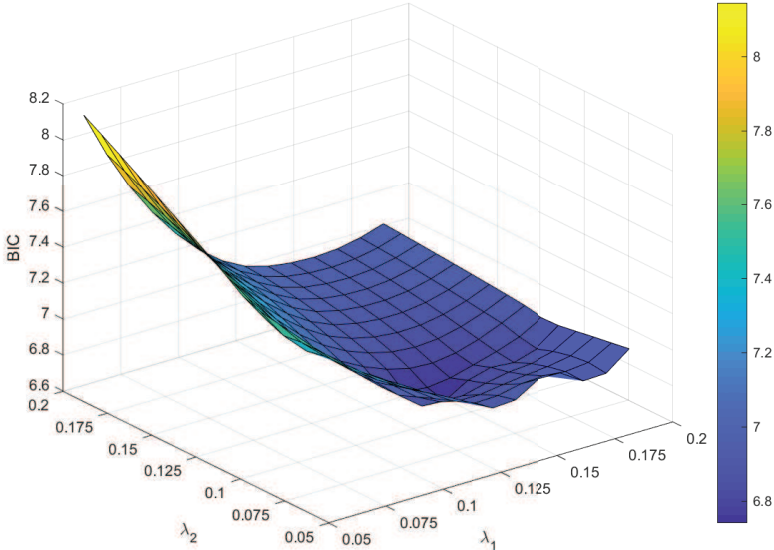


Figure A1: Simulation: BIC as a function of λ_1 and λ_2

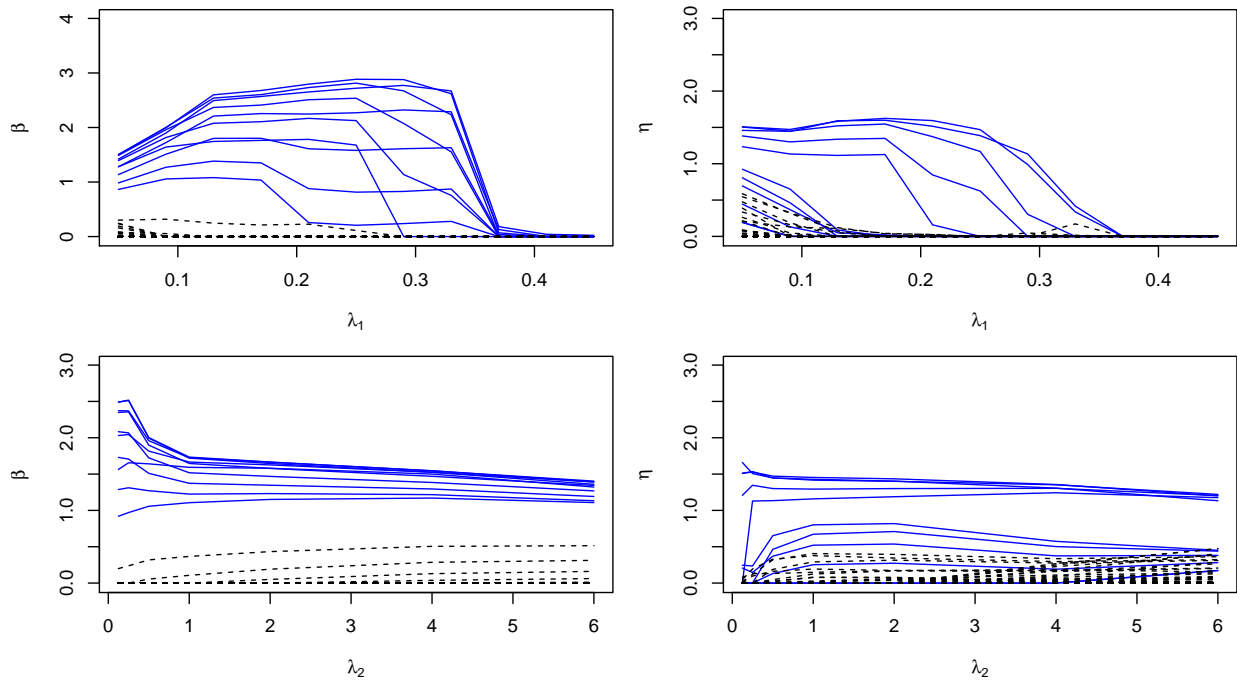


Figure A2: Simulation: parameter paths for one replicate under the linear model with MAF setting M1 and correlation structure AR(0.3). The blue solid lines represent the first ten true positives, and the black dashed lines represent the true negatives.

Table A1: Simulation results under the AFT model with MAF setting M1. In each cell, mean (sd) based on 500 replicates.

	M:TP	M:FP	I:TP	I:FP	RSSE	RSE	Cstat
AR(0.3)							
MA	0.8(1.7)	40.3(38.0)	2.8(2.8)	95.5(77.6)	14.05(4.77)	26.37(19.93)	0.74(0.05)
HierMCP	13.5(1.9)	38.3(6.3)	0.8(0.9)	0.5(0.8)	9.72(0.57)	15.84(1.81)	0.81(0.03)
SMCP	4.8(4.8)	6.5(13.7)	9.1(6.6)	31.9(15.7)	8.54(0.56)	3.24(0.80)	0.85(0.03)
Proposed	19.2(1.2)	1.2(6.7)	33.1(6.1)	6.1(4.3)	2.99(1.09)	2.29(0.72)	0.93(0.02)
AR(0.5)							
MA	1.8(2.7)	55.8(38.9)	4.7(4.0)	127.3(75.0)	71.88(62.71)	173.12(166.62)	0.56(0.10)
HierMCP	12.9(1.8)	40.6(6.9)	0.9(1.0)	0.9(0.9)	10.13(0.69)	17.32(2.16)	0.80(0.03)
SMCP	6.5(4.9)	7.9(12.9)	8.9(7.2)	34.4(16.3)	8.36(0.72)	3.50(0.91)	0.85(0.03)
Proposed	19.3(1.3)	0.4(2.3)	34.2(4.9)	5.4(4.0)	2.82(1.02)	2.18(0.58)	0.93(0.01)
Band1							
MA	1.1(1.9)	41.6(42.5)	2.5(2.6)	92.7(80.5)	13.71(4.68)	25.49(20.59)	0.72(0.08)
HierMCP	13.5(1.7)	37.1(5.7)	0.7(0.7)	0.4(0.8)	9.66(0.51)	15.60(1.67)	0.81(0.03)
SMCP	4.6(4.7)	5.1(12.0)	9.2(6.5)	28.5(15.6)	8.51(0.65)	3.20(0.92)	0.86(0.03)
Proposed	19.3(1.2)	0.4(1.4)	33.4(5.4)	6.1(4.9)	2.92(0.90)	2.25(0.76)	0.93(0.01)
Band2							
MA	1.8(2.3)	59.6(41.1)	5.5(3.9)	131.5(73.7)	100.86(90.94)	245.78(233.22)	0.54(0.07)
HierMCP	12.8(1.9)	42.0(8.2)	1.2(1.0)	0.6(0.8)	10.19(0.76)	17.70(2.15)	0.80(0.03)
SMCP	9.4(5.2)	17.8(18.5)	9.3(6.5)	35.8(14.1)	8.10(0.83)	4.00(1.01)	0.85(0.03)
Proposed	19.0(2.3)	1.6(7.1)	33.2(7.5)	5.5(4.9)	2.97(1.46)	2.24(0.90)	0.93(0.02)
LD(0.3)							
MA	1.5(2.6)	48.4(42.2)	4.1(3.5)	103.0(78.6)	17.58(8.62)	37.39(34.40)	0.70(0.09)
HierMCP	13.4(2.0)	50.4(8.2)	0.6(0.9)	0.2(0.6)	10.58(0.81)	18.96(2.47)	0.80(0.03)
SMCP	4.4(4.5)	4.7(11.7)	11.7(8.1)	21.3(11.2)	8.33(0.88)	2.98(0.67)	0.86(0.03)
Proposed	19.2(1.6)	0.3(1.5)	34.0(5.7)	4.6(3.2)	2.79(1.04)	2.11(0.68)	0.93(0.01)
LD(0.5)							
MA	2.1(3.1)	57.5(39.7)	7.3(4.9)	121.8(70.1)	49.40(40.45)	125.38(118.24)	0.58(0.10)
HierMCP	12.6(2.1)	55.4(9.6)	0.8(0.8)	0.3(0.6)	11.18(0.90)	21.26(2.79)	0.78(0.07)
SMCP	6.8(5.7)	8.0(13.8)	13.8(8.6)	22.7(12.9)	7.87(1.02)	3.16(1.04)	0.85(0.08)
Proposed	19.4(1.1)	0.2(1.8)	34.1(4.7)	4.8(3.9)	2.78(0.89)	2.10(0.60)	0.93(0.02)

Table A2: Simulation results under the AFT model with MAF setting M2. In each cell, mean (sd) based on 500 replicates.

	M:TP	M:FP	I:TP	I:FP	RSSE	RSE	Cstat
AR(0.3)							
MA	2.1(2.7)	60.5(28.0)	5.4(3.8)	157.2(67.9)	145.73(130.23)	360.20(327.86)	0.55(0.04)
HierMCP	13.6(1.9)	34.5(6.7)	1.2(1.1)	0.7(0.9)	9.56(0.60)	15.53(2.01)	0.82(0.03)
SMCP	5.8(4.8)	9.4(15.1)	4.1(2.7)	81.9(20.0)	8.68(0.37)	3.47(0.57)	0.82(0.05)
Proposed	18.8(2.0)	8.1(17.1)	30.1(9.9)	6.5(4.1)	3.52(1.74)	2.66(1.07)	0.92(0.03)
AR(0.5)							
MA	3.2(3.5)	68.6(21.8)	7.8(4.9)	172.3(47.2)	184.51(107.73)	451.07(267.52)	0.53(0.04)
HierMCP	12.8(1.8)	37.9(7.4)	1.2(1.2)	0.9(0.9)	10.05(0.75)	17.06(2.41)	0.80(0.03)
SMCP	7.3(5.0)	12.4(18.1)	3.8(3.3)	80.6(20.1)	8.56(0.53)	3.60(0.55)	0.82(0.03)
Proposed	18.9(2.2)	6.5(19.5)	31.9(9.4)	5.6(4.9)	3.22(1.80)	2.37(0.97)	0.92(0.03)
Band1							
MA	2.2(2.8)	61.6(33.5)	5.1(3.8)	151.4(71.4)	135.71(124.35)	330.96(314.37)	0.52(0.05)
HierMCP	13.8(1.7)	33.5(6.0)	1.3(1.1)	0.7(0.7)	9.45(0.55)	15.20(1.91)	0.82(0.03)
SMCP	6.3(4.7)	8.0(13.0)	4.0(3.2)	79.8(19.9)	8.62(0.42)	3.40(0.51)	0.84(0.02)
Proposed	18.9(1.7)	14.8(28.5)	28.3(11.3)	6.3(4.6)	3.87(1.99)	2.82(1.22)	0.91(0.03)
Band2							
MA	3.8(3.6)	64.9(24.8)	8.8(4.7)	167.1(51.5)	207.33(179.97)	519.71(455.48)	0.53(0.04)
HierMCP	12.6(1.8)	38.8(8.1)	1.6(1.3)	1.0(1.0)	10.11(0.75)	17.74(2.17)	0.80(0.03)
SMCP	8.0(4.5)	12.8(17.4)	3.6(3.2)	79.5(21.2)	8.56(0.49)	3.71(0.62)	0.82(0.03)
Proposed	18.5(2.8)	11.3(24.1)	29.4(11.5)	5.5(4.0)	3.67(2.08)	2.65(1.26)	0.91(0.03)
LD(0.3)							
MA	1.5(2.6)	48.4(42.2)	4.1(3.5)	103.0(78.6)	17.58(8.62)	37.39(34.40)	0.70(0.09)
HierMCP	13.4(2.0)	50.4(8.2)	0.6(0.9)	0.2(0.6)	10.58(0.81)	18.96(2.47)	0.80(0.03)
SMCP	3.9(4.1)	3.0(8.4)	11.8(8.3)	20.6(10.6)	8.36(0.87)	2.91(0.63)	0.86(0.03)
Proposed	19.2(1.6)	0.3(1.5)	34.0(5.7)	4.6(3.2)	2.79(1.04)	2.11(0.68)	0.93(0.01)
LD(0.5)							
MA	2.1(3.1)	57.5(39.7)	7.3(4.9)	121.8(70.1)	49.40(40.45)	125.38(118.24)	0.58(0.10)
HierMCP	12.6(2.1)	55.4(9.6)	0.8(0.8)	0.3(0.6)	11.18(0.90)	21.26(2.79)	0.78(0.07)
SMCP	6.7(5.6)	7.6(13.6)	13.8(8.6)	22.6(12.9)	7.89(1.00)	3.15(1.04)	0.85(0.08)
Proposed	19.4(1.1)	0.2(1.8)	34.1(4.7)	4.8(3.9)	2.78(0.89)	2.10(0.60)	0.93(0.02)

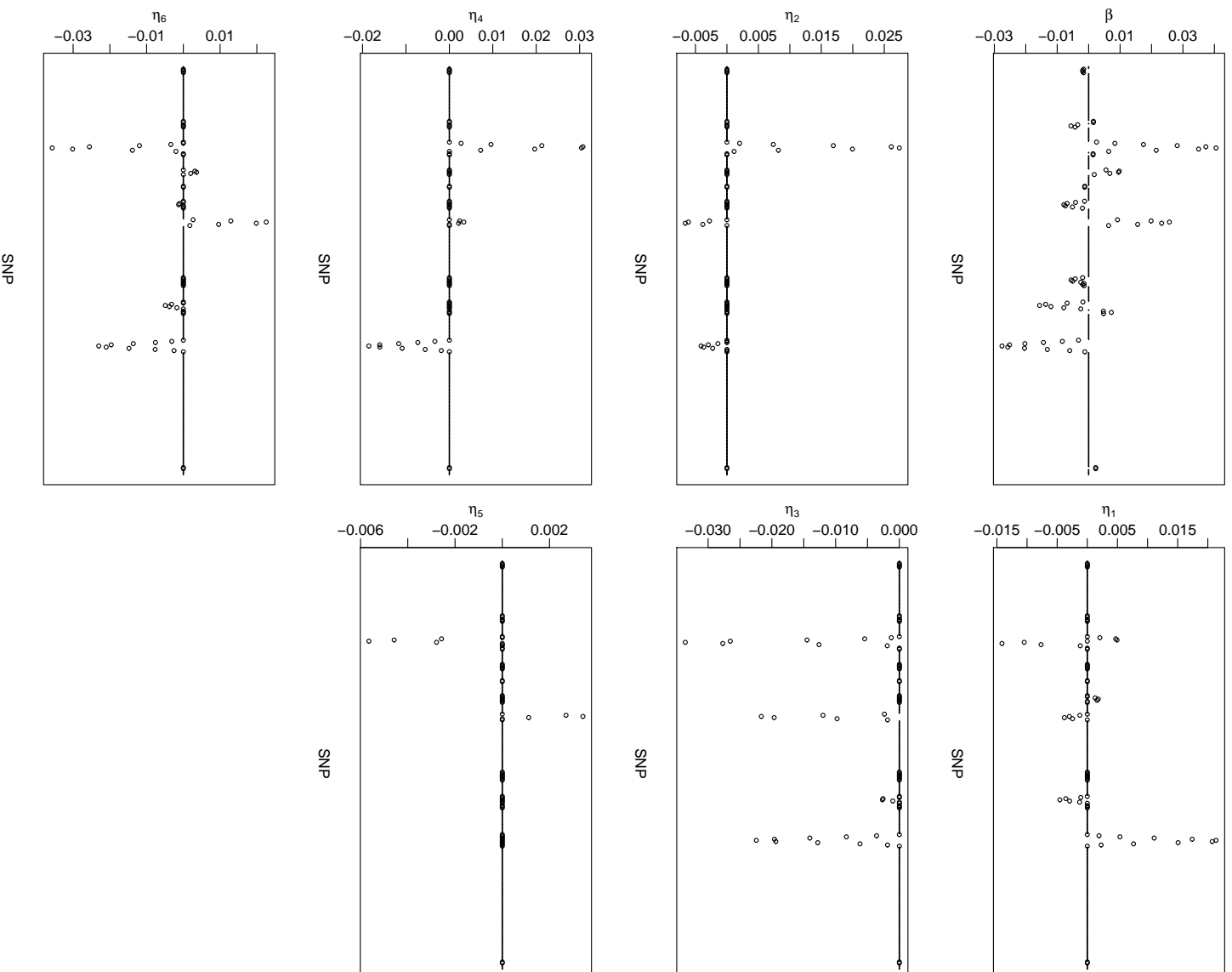


Figure A3: Analysis of the GENEVA diabetes data (NHS/HPFS) using the proposed approach: identified main G effects and interactions.

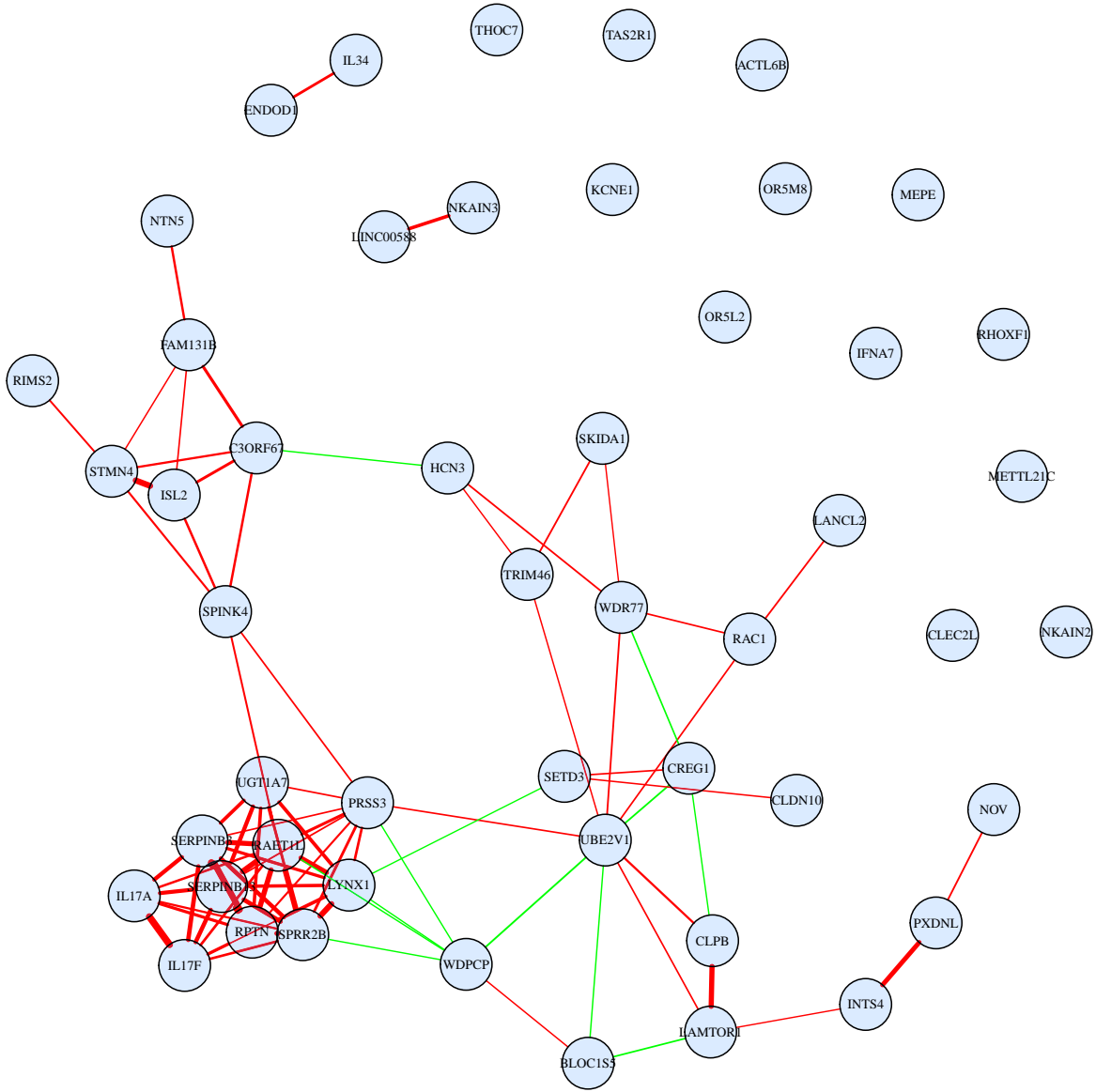


Figure A4: Analysis of the TCGA SKCM data using the proposed approach: identified main G effects. The edges between genes are defined based on the values of a_{jl} 's of the adjacency matrix $\mathbf{A} = (a_{jl})_{p \times p}$. Positive and negative connections are represented with red and green, respectively. The thickness (strength) of an edge is proportional to $|a_{jl}|$.

Table A3: Data analysis: numbers of main G effects and interactions identified by different approaches and their overlaps.

GENEVA	Main				Interaction			
	MA	HierMCP	SMCP	Proposed	MA	HierMCP	SMCP	Proposed
MA	51	10	33	32	57	0	31	0
HierMCP		67	8	6		158	0	5
SMCP			41	30			156	0
Proposed				71				128

SKCM	Main				Interaction			
	MA	HierMCP	SMCP	Proposed	MA	HierMCP	SMCP	Proposed
MA	27	3	0	0	21	0	0	0
HierMCP		130	1	1		78	0	0
SMCP			39	15			34	5
Proposed				50				44